



This is a repository copy of *Application of scattering and diffraction techniques for the morphological characterization of asphaltenes*.

White Rose Research Online URL for this paper:

<https://eprints.whiterose.ac.uk/196073/>

Version: Accepted Version

Article:

Jennings, J., Growney, D.J., Brice, H. et al. (2 more authors) (2022) Application of scattering and diffraction techniques for the morphological characterization of asphaltenes. *Fuel*, 327. 125042. ISSN 0016-2361

<https://doi.org/10.1016/j.fuel.2022.125042>

Article available under the terms of the CC-BY-NC-ND licence
(<https://creativecommons.org/licenses/by-nc-nd/4.0/>).

Reuse

This article is distributed under the terms of the Creative Commons Attribution-NonCommercial-NoDerivs (CC BY-NC-ND) licence. This licence only allows you to download this work and share it with others as long as you credit the authors, but you can't change the article in any way or use it commercially. More information and the full terms of the licence here: <https://creativecommons.org/licenses/>

Takedown

If you consider content in White Rose Research Online to be in breach of UK law, please notify us by emailing eprints@whiterose.ac.uk including the URL of the record and the reason for the withdrawal request.



eprints@whiterose.ac.uk
<https://eprints.whiterose.ac.uk/>



This is a repository copy of *Application of scattering and diffraction techniques for the morphological characterization of asphaltenes*.

White Rose Research Online URL for this paper:

<https://eprints.whiterose.ac.uk/196073/>

Version: Published Version

Article:

Jennings, J., Growney, D.J., Brice, H. et al. (2 more authors) (2022) Application of scattering and diffraction techniques for the morphological characterization of asphaltenes. *Fuel*, 327. 125042. p. 125042. ISSN 0016-2361

<https://doi.org/10.1016/j.fuel.2022.125042>

Reuse

Items deposited in White Rose Research Online are protected by copyright, with all rights reserved unless indicated otherwise. They may be downloaded and/or printed for private study, or other acts as permitted by national copyright laws. The publisher or other rights holders may allow further reproduction and re-use of the full text version. This is indicated by the licence information on the White Rose Research Online record for the item.

Takedown

If you consider content in White Rose Research Online to be in breach of UK law, please notify us by emailing eprints@whiterose.ac.uk including the URL of the record and the reason for the withdrawal request.



eprints@whiterose.ac.uk
<https://eprints.whiterose.ac.uk/>

1 **Application of scattering and diffraction techniques for the morphological**
2 **characterization of asphaltenes**

3

4 J. Jennings^{1*}, D. J. Gowney², H. Brice², O. O. Mykhaylyk¹, S. P. Armes¹

5 ¹Dainton Building, Chemistry Department, The University of Sheffield, Sheffield, South Yorkshire, S3
6 7HF, UK.

7 ²Lubrizol Ltd, Nether Lane, Hazelwood, Derbyshire DE56 4AN, UK.

8 **Keywords:** Asphaltenes, Small Angle X-ray Scattering, Small Angle Neutron Scattering, Diffraction,
9 Colloids

10 **Abstract.** Asphaltenes are an important class of complex carbon-rich molecules found in crude oil.
11 Their chemical structure varies depending on the geological source but generally comprises fused
12 aromatic rings, aliphatic substituents and heteroatom functionality, which results in a strong tendency
13 to aggregate and phase separate within crude oil. Asphaltene ‘drop-out’ owing to phase separation is a
14 major problem spanning crude oil extraction, refining and application. More specifically, the build-up
15 of asphaltene deposits can reduce the permeability of porous rock formations, block oil pipelines, and
16 compromise the efficiency of marine engines. This major technical problem is compounded by the fact
17 that the chemical composition, structure and colloidal behavior of asphaltenes varies significantly
18 depending on the origin of the crude oil and the conditions employed for its refinement. As a result,
19 there has been a concerted effort to (i) understand the morphology of asphaltene dispersions, (ii) identify
20 the underlying mechanism(s) that lead to asphaltene ‘drop-out’ and hence (iii) design stabilizers to
21 maintain colloid stability and/or minimize ‘drop-out’. In principle, imaging techniques can be used to
22 visualize the asphaltene aggregates while light scattering can provide particle size information, but these
23 techniques only provide rather limited structural information. Asphaltene aggregation involves several
24 steps and results in highly hierarchical structures including primary nanoaggregates, clusters, and fractal
25 structures, with characteristic length scales ranging from a few angstroms to several microns. In this
26 review article, the use of small-angle scattering (SAS) and X-ray diffraction (XRD) to characterize
27 asphaltene powders, dispersions and aggregates over the past six decades is summarized. These
28 powerful techniques provide a wealth of structural information about molecular stacking, particle size
29 and morphology, and fractal dimensions.

30

31 * Author to whom correspondence should be addressed, james.jennings@uni-graz.at

32

33

34 **The chemistry of asphaltenes**

35 Asphaltenes comprise the fraction of crude oil that contains the most polar and unsaturated
36 molecules, which are often referred to as ‘vacuum residues’ owing to their relatively high boiling
37 points.^{1, 2} The chemical structures within this fraction are complex, highly polydisperse, difficult to
38 separate, and vary widely depending on the geographical source of the crude oil and the precise
39 conditions used for its cracking and fractionation.³ In general, the physical properties of asphaltenes
40 (e.g. very high viscosity, high density, low solubility in crude oil, etc.) are governed by their
41 polyaromatic chemical structure (Figure 1).⁴ Asphaltenes have long been considered to comprise dense
42 polyaromatic regions that are either arranged as one continuous ‘island’, or as multiple polyaromatic
43 rings connected by saturated hydrocarbon linkages known as an ‘archipelago’ topology (Figure 1A).⁵
44 Recently, direct imaging of asphaltene using atomic force microscopy revealed that ‘island-like’
45 molecules tend to be the major component.⁶

46 Asphaltenes are typically characterized by their mean chemical composition. For example, the
47 hydrogen/carbon (H/C) ratio indicates the degree of saturation, with lower H/C values being
48 characteristic of predominantly aromatic-rich molecules and higher H/C values for aliphatic-rich
49 systems. Another important aspect is the fraction and type of heteroatoms (particularly oxygen, nitrogen
50 and sulfur) that are present in the form of various functional groups such as carboxylic acids, esters,
51 alcohols, ketones, amines, amides, pyrroles, pyridines, (di)sulfides, thiophenes, and sulfoxides.^{7, 8}
52 Average chemical compositions can be obtained from elemental analysis and NMR spectroscopy, and
53 functional groups can be analyzed by FTIR and X-ray Photoelectron Spectroscopy (XPS). However,
54 these variables alone do not predictably govern the physical properties of asphaltenes.

55 Mass spectrometry studies indicate that asphaltenes contain remarkably broad range of
56 chemical structures, both in terms of molecular weight and functionality.^{1, 2, 9} However, the organic
57 chemistry of asphaltenes lies outside of the scope of this review article. Instead, we focus on the
58 essential structural features that account for its complex colloidal morphology. There is a large body of
59 empirical evidence to suggest that asphaltenes exist within crude oil as stable colloids,¹⁰⁻¹² although
60 there is some debate regarding both size and shape of dispersed asphaltene particles.⁵ Aromatic-rich

61 asphaltenes are expected to have low solubility in the more aliphatic-rich fractions of crude oil, such as
62 the maltenes.² However, naturally-occurring crude oil fractions known as ‘resins’ are believed to aid
63 the stabilization of asphaltenes in the form of suspensions.³ Relatively small changes in solution
64 temperature, solvent composition, pressure or dissolved gases can affect the colloidal stability of
65 asphaltenes within crude oil, leading to macroscopic phase separation – otherwise known as ‘drop-out’
66 – that leads to a multitude of industrial problems.⁵

67 At a molecular level, intermolecular π - π^* interactions between polyaromatic regions of
68 asphaltenes lead to the formation of stacks of aromatic layers similar to graphite that are referred to as
69 primary nanoaggregates, crystallites, or micelles (Figure 1B). These stacks can undergo further
70 aggregation to form macroscopic precipitates that lead to engine fouling or pipe blockages. The
71 mechanism of asphaltene aggregation was first described by the Yen-Mullins model, although our
72 understanding of this process has evolved over the last 50 years.^{5, 11-14} Various studies have sought to
73 describe asphaltene drop-out in terms of a liquid-liquid phase separation process, particularly under
74 high temperature and pressure conditions.^{15, 16}

75 Despite their structural complexity at the molecular level, it is widely accepted that the physical
76 behavior of asphaltenes can be understood by characterizing their morphology over multiple length
77 scales, rather than by attempting to catalogue their many molecular components.⁵ Thus, asphaltene
78 dispersions are often described in terms of their radius of gyration (R_g) and molecular weight (M_w),
79 which denotes their mean cluster size (at one or more length scales) and average number of molecules
80 per cluster, respectively. Indeed, specific chemical functionalities can induce subtle changes in
81 intermolecular interactions that either promote or inhibit aggregation (e.g. heteroatom content^{8, 17}).
82 Correlation of data collected from molecular and colloidal analyses can, therefore, provide powerful
83 insight into the driving forces for the aggregation processes.

84

85

86

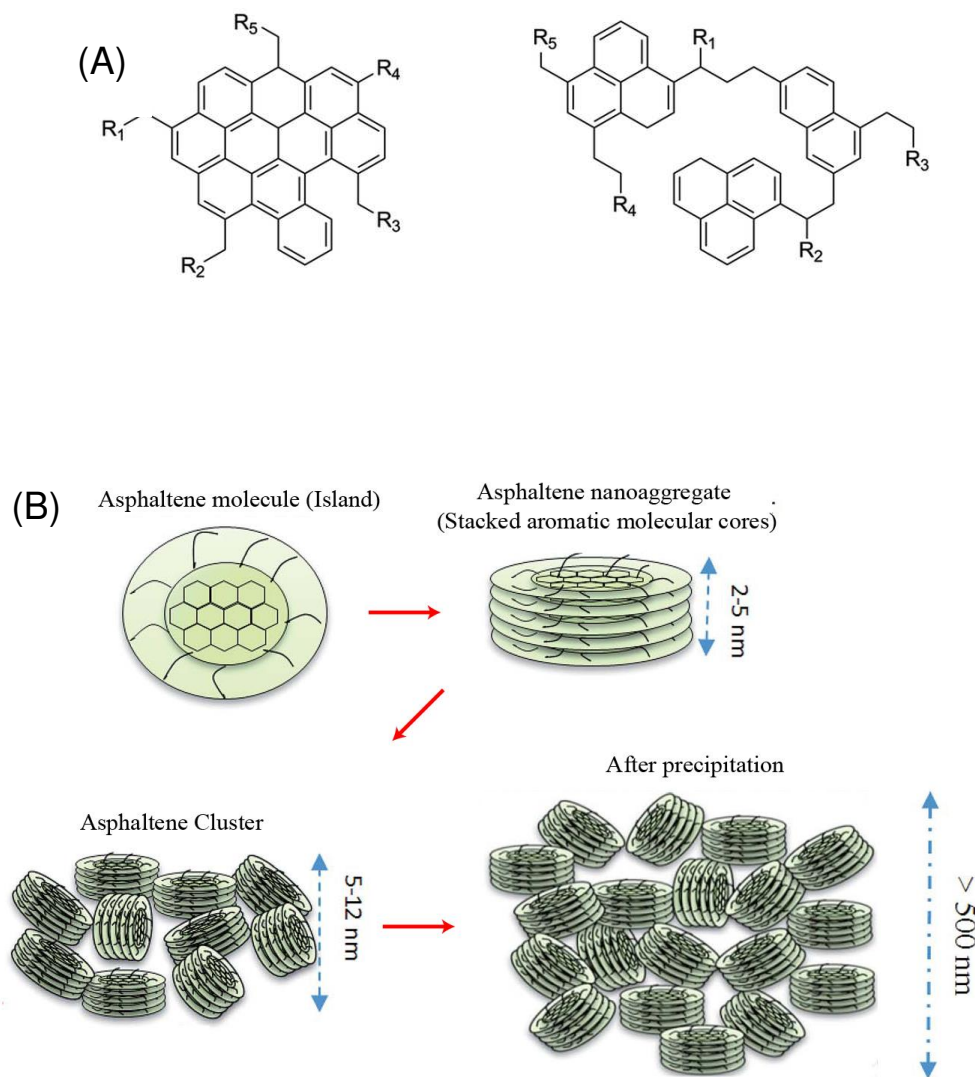
87

89

90

91

92



93

94 **Figure 1.** (A) Examples of chemical structures found within asphaltene mixtures: single fused aromatic

95 cores (left, "island" topology) or multiple aromatic cores interconnected by aliphatic spacers (right,

96 "archipelago" topology). (B) Schematic representation of the Yen-Mullins model of asphaltene

97 aggregation, one theory that describes asphaltene phase separation (adapted from the literature).^{5, 11-14,}

98 18

99 **Problems and opportunities arising from asphaltene aggregation**

100 Asphaltene 'drop-out' causes huge problems across multiple industrial sectors and at every

101 stage of the supply chain. For example, at the stage of enhanced oil recovery, dissolution of light gases

102 within crude oil can cause asphaltene deposition onto porous rock formations and tubing, leading to

103 environmental problems and production losses for oil wells.^{10, 19} Similarly, diluents are often required
104 for downstream crude oil processing, and the corresponding change in solvency sometimes leads to
105 asphaltene fouling of machinery.²⁰ In the case of fuel transportation, mixing oils from various sources
106 with differing compositions can lead to significant pipeline blockages owing to asphaltene ‘drop-out’.⁴
107 ²¹ In general, phase separation of asphaltenes may be triggered when (i) the overall solvent quality
108 changes leading to a reduction in the Hildebrand solubility parameter (δ) (e.g. by introducing an
109 aliphatic-rich solvent),²² (ii) there is a significant change in temperature,²³ or (iii) there is dissolution of
110 gaseous lower alkanes or CO₂ within crude oil.²⁴

111 Although asphaltene ‘drop-out’ is clearly undesirable in many cases, the viscoelastic properties
112 conferred by asphaltene as a result of its complex morphology of colloidal aggregates has been
113 traditionally exploited to produce useful materials for road surfaces.²⁵ In this case, asphaltenes (and
114 other crude oil fractions) act as a binder for the sand and stone particulates that comprise most of the
115 ‘asphalt’ formulation. More recently, various research groups have evaluated asphaltenes (and
116 polyaromatic hydrocarbons in general) in the context of organic dye sensitized solar cells²⁶,
117 supercapacitors,²⁷ biological imaging,²⁸ and electrocatalysis.²⁹ The properties that arise from the highly
118 conjugated polyaromatic ring systems enable these technologies, allowing the molecules to interact with
119 light at multiple wavelengths and effectively conduct electrons.³⁰ In principle, understanding the
120 colloidal aggregation of asphaltenes may not only prevent machinery fouling and pipeline blockages
121 but could also be desirable for future materials applications.³¹

122 **Analyzing the hierarchical structure of asphaltene aggregates**

123 Asphaltene forms hierarchical structures comprising fractal clusters that are in turn made up of
124 ‘nanoaggregates’ composed of a few individual asphaltene molecules (Figure 1B). Therefore, the
125 rigorous characterization of asphaltene dispersions requires analysis over multiple length scales using
126 a range of techniques, including light microscopy, electron microscopy, dynamic light scattering (DLS),
127 small-angle X-ray and neutron scattering (SAXS and SANS), and X-ray diffraction (XRD). Primary
128 asphaltene nanoaggregates of 1 to 10 nm are technically challenging to image by transmission or
129 scanning electron microscopy (TEM or SEM). However, AFM imaging has been used to visualize

130 individual molecules.⁶ Higher order fractal clusters of asphaltenes possess length scales ranging from
131 10 nm to several microns can be observed by electron microscopy¹⁸ but drying artefacts may affect the
132 (apparent) extent of asphaltene aggregation, while the ultrahigh vacuum conditions preclude *in situ*
133 studies. However, these limitations may be overcome by adopting sophisticated techniques such as
134 cryo-TEM³² and so-called ‘liquid cell’ TEM.³³ In addition, such imaging techniques invariably suffer
135 from poor sampling statistics: only a few hundred particles are typically analyzed, and thus the data
136 may not be truly representative of the whole sample.

137 Clearly, many of the industrial problems associated with asphaltenes arise from their phase
138 separation from crude oil. Thus, monitoring the kinetics of this process is of considerable interest.
139 Techniques that enable *in situ* analysis of the evolution in colloidal morphology under industrially-
140 relevant conditions are particularly informative. The kinetics of aggregation can be monitored
141 spectroscopically using techniques that distinguish between dispersed and insoluble asphaltene
142 fractions. For example, the absorption recorded at 400 nm using uv-visible absorption spectroscopy is
143 proportional to the concentration of ‘dissolved’ asphaltenes,³⁴ while optical microscopy can provide
144 insight into the relatively large asphaltene particles (i.e. > 500 nm diameter) that can form during the
145 latter stages of precipitation.³⁵ However, although useful for initial screening experiments, these
146 techniques lack the resolution required to detect structural organization at atomic and molecular scales
147 and the primary clusters that are formed during the onset of aggregation.

148 Scattering methods overcome many of the limitations of the other outlined techniques: *in situ*
149 analysis across multiple length scales can be conducted on many millions of particles and hence offer
150 far more reliable statistics. In principle, DLS can yield valuable data when studying the kinetics of
151 asphaltene particle size growth.³⁶ However, it does not provide insights into structural morphologies.
152 Thus, this review focuses on the use of X-ray and neutron scattering and diffraction for asphaltene
153 characterization because such techniques can provide rich structural information over multiple length
154 scales of hierarchical asphaltene organization. Solid-state NMR spectroscopy can also provide useful
155 physical insights regarding asphaltene aggregation by probing π - π stacking interactions.³⁷

156 Several recent review articles focus on various aspects of asphaltene aggregation, often from an
157 industrial perspective.^{4, 5, 11, 12, 19, 22, 38} Of the various characterization techniques that have been used to
158 study the morphology of asphaltenes, SAXS and/or SANS provide particularly useful information on
159 the morphology of asphaltenes over multiple length scales (1 Å to 1 μm), whilst XRD allows
160 exploration of the sub-nm intermolecular packing. This review article focuses on summarizing the
161 relevant literature that has informed our understanding of the mechanism of phase separation, likely
162 aggregate morphologies, and the physicochemical properties of asphaltenes. Data interpretation can be
163 an issue in scattering experiments because sometimes more than one model can be applied to fit a given
164 scattering pattern. Thus, we also compare the various modelling approaches that have been applied. By
165 compiling the structural information acquired to date, we hope to facilitate the design of new scattering
166 experiments to study asphaltene phase separation processes.

167 **Morphological studies using X-ray scattering and diffraction techniques**

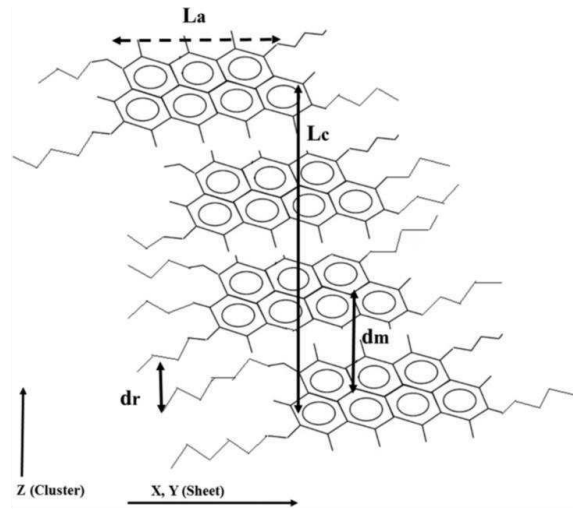
168 ***XRD***

169 X-rays can provide detailed information on molecular length scales within primary asphaltene
170 particles by studying their diffraction from asphaltene powders or dispersions at wide angles (i.e. $2\theta >$
171 10° for the characteristic X-ray radiation of a copper anode). In general terms this technique is called
172 wide-angle X-ray scattering (WAXS) which also includes diffraction as a special case of scattering.
173 The latter is usually distinguished as a separate technique called either wide-angle X-ray diffraction
174 (WAXD) or, more commonly, XRD. Although asphaltenes are classified as amorphous carbons,^{39, 40}
175 diffraction occurs as a result of the regular packing of asphaltenes within primary nanoaggregates.
176 While discussing WAXS and XRD, for the sake of both simplicity and consistency with the literature,
177 the term XRD will be used in this review. XRD can be used to determine morphological parameters for
178 asphaltene particles by analyzing the position, width and relative area of diffraction peaks (see Figure
179 2 for a schematic description of these parameters).³⁹ XRD patterns of asphaltenes typically consist of
180 two groups of peaks, one of which arises from the stacked polyaromatic cores and the other, called γ -
181 band, from the packed aliphatic chains. In an analogy to structures formed by stacked aromatic rings,
182 the first group of asphaltene XRD peaks is represented by 002 and, sometimes, 004 reflections assigned

183 by Miller indices corresponding to hexagonal graphite structure and associated with (00*l*) basal planes
184 formed by graphene-like layers, as well as by two-dimensional *hk* diffuse bands such as 10 and 11 bands
185 assigned similarly to *hk0* reflections of graphite crystal structure.⁴¹

186 The *q* value for the 002 peak maximum (q_{002}) can be used to calculate the mean spacing between
187 aromatic cores (d_m) using the relation $d_m = \frac{2\pi}{q_{002}}$. Meanwhile, the *q* position of the γ -band (q_{\max}) can be
188 used to estimate the mean distance between aliphatic chains (d_r) at the periphery of asphaltene particles
189 from the relation $d_r = \frac{2\pi}{q_{\max}}$. The relative areas of these two peaks also provides an estimate for the
190 aromatic fraction (f_a) within a given asphaltene sample. Analyzing a full width at half maximum of the
191 002 peak ($fwhm_{002}$) using the Scherrer equation, allows the mean thickness of asphaltene clusters (L_c)
192 to be estimated by $L_c = \frac{0.45}{fwhm_{002}}$ (Figure 2). This parameter can then be correlated with the number of
193 asphaltene molecules within a stack (M_e) by relating to d_m (Figure 2). Finally, the mean aggregate stack
194 diameter (L_a), which is related to the size of the aromatic cores within the asphaltene, can be calculated
195 from *fwhm* of the 11 band ($fwhm_{11}$) by $L_a = \frac{0.92}{fwhm_{11}}$.

196



$$f_a = \frac{A_{002}}{A_{002} + A_r} \quad d_m = \frac{2\pi}{q_{002}} \quad d_r = \frac{2\pi}{q_\gamma}$$

$$L_c = \frac{0.45}{fwhm_{002}} \quad M_e = \frac{L_c}{d_m} + 1 \quad L_a = \frac{0.92}{fwhm_{11}}$$

A_x = area of peak x

q_x = q position of peak x (in \AA^{-1})

$fwhm_x$ = full width at half maximum of peak x

197

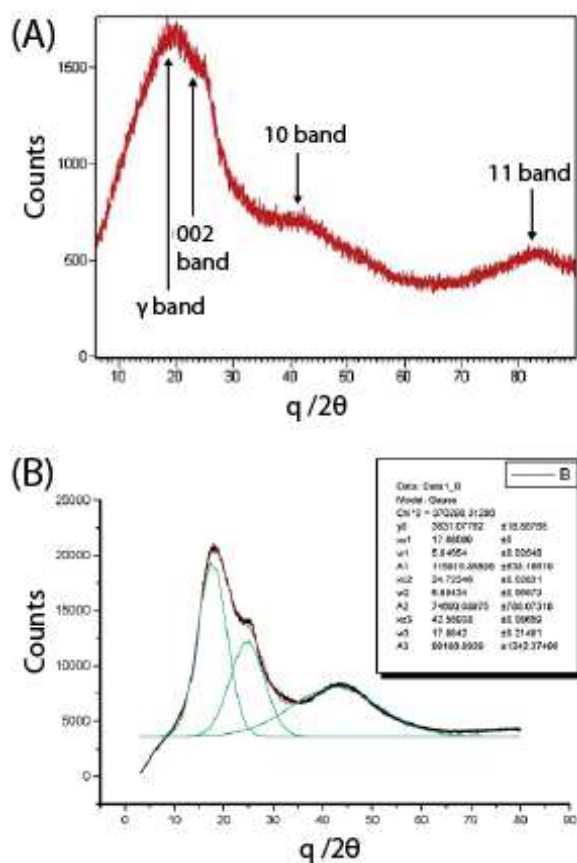
198 **Figure 2.** Schematic representation of the features of asphaltene clusters that can be resolved using
 199 XRD: L_a is the mean diameter of the aromatic core; L_c is the mean thickness of an aromatic stack (which
 200 is proportional to the number of asphaltene molecules within a stack, M_e); d_m is the mean distance
 201 between aromatic cores; d_r is the mean distance between aliphatic chains on the periphery of the
 202 asphaltene stacks. Equations on the right are those applied to XRD data in order to obtain estimates for
 203 these structural parameters.

204

205 The XRD data analysis above was originally developed to characterize a range of amorphous
 206 carbon structures such as carbon black and coals.⁴² Assuming similarities of the structures, it has
 207 subsequently been adapted to characterize asphaltene XRD data, mostly in the solid powder form
 208 (Figure 3).^{18, 39, 43-58} Peak-fitting functions are usually used to deconvolute XRD patterns into an

209 appropriate diffraction peaks/diffuse bands (Figure 3C) in order to determine asphaltene structural
210 parameters (Figure 2). The literature data calculated from such analyses are summarized in Table 1.

211



212

213

214 **Figure 3.** (A) Typical XRD data recorded for asphaltenes in the solid state, illustrating 002 peak arising
215 from aromatic stacks and γ -band from average distances between aliphatic chains, with 10 and 11 bands
216 also visible at higher scattering angles.⁵³ (B) Example of a peak fitting protocol applied to an XRD
217 pattern.⁴⁹

218

219

220

221

Table 1. Summary of stack diameters (L_a), stack thicknesses (L_c), interlayer spacings (d_m) and aliphatic distances (d_r) derived from analysis of XRD data reported in the literature.

Entry & reference	Publication Year	Variables studied	$L_a/\text{Å}$	$L_c/\text{Å}$	$d_m/\text{Å}$	$d_r/\text{Å}$	M_c
1 ³⁹	1961	Oil Source	10.0 – 17.0	17.0 – 20.0	3.57 – 3.60	4.60 – 4.90	n/a
2 ⁴³	1983	Oil Source	8.0 – 10.3	10.3 – 13.6	3.60 – 3.70	4.40 – 5.20	3.9 – 4.8
3 ⁴⁴	1996	Oil Source	12.2 – 18.1	21.8 – 22.2	3.54 – 3.57	4.31 – 4.47	6.1 – 6.3
4 ⁴⁵	1997	Oil Source	11.9 – 13.0	22.7 – 24.7	3.60	4.40 – 4.50	7.4 – 8.0
5 ⁴⁶	2002	Oil Source	9.9 – 11.0	14.3 – 25.2	3.50 – 3.70	5.60 – 6.20	4.9 – 8.2
		Reaction Condition	7.0 – 9.5	22.4 – 27.6	3.50 – 3.60	4.50 – 5.90	7.2 – 8.9
6 ⁴⁷	2004	Oil Source	13.1 – 16.6	23.7 – 25.4	3.51 – 3.56	4.37 – 4.40	6.7 – 7.1
		Fraction	12.9 – 14.2	26.5 – 31.2	3.52 – 3.54	4.10 – 4.32	7.4 – 8.9
7 ⁴⁸	2004	Oil Source	n/a	25.2 – 25.9	3.53	n/a	8.2 – 8.4
		Temperature	n/a	13.7 – 25.2	3.53 – 3.62	n/a	4.8 – 8.2
8 ⁴⁹	2005	Oil Source	11.1 – 16.7	16.3 – 32.7	3.49 – 3.51	4.32 – 4.90	n/a
		Fraction	10.4 – 12.8	16.3 – 19.4	3.44 – 3.52	4.25 – 4.69	n/a
9 ⁵⁰	2007	Reaction condition (pressure)	n/a	33.5 – 35.6	3.51 – 3.58	n/a	10.4 – 10.6
		Reaction condition (temperature)	n/a	26.3 – 33.5	3.53 – 3.60	n/a	8.3 – 10.6
		Reaction condition (flow)	n/a	31.7 – 34.9	3.48 – 3.60	n/a	10.1 – 10.7
10 ⁵¹	2007	None	17.6	28.2	3.56	4.35	8.0
11 ⁵²	2013	Oil Source	n/a	n/a	3.45 – 3.52	4.87 – 5.13	n/a
		Solvent	n/a	n/a	3.45 – 3.49	4.87 – 7.71	n/a
12 ⁵⁹	2013	Method	3.6 – 4.7	3.6 – 5.2	4.00 – 4.70	6.00 – 8.00	1.8 – 2.3
		Oil Source	3.2 – 5.6	3.6 – 7.7	4.30 – 4.70	6.60 – 8.00	1.8 – 2.8
13 ⁵³	2015	Oil Source	7.2 – 8.2	12.1 – 15.0	3.50	4.60 – 4.70	5.0

		Reaction condition	6.9 – 8.0	7.8 – 14.0	3.50 – 3.70	4.70 – 5.50	3.0 – 5.0
14 ⁵⁴	2016	Fraction	n/a	18.0 – 48.0	3.43 – 3.57	4.06 – 4.49	7.0 – 15.0
15 ⁵⁵	2016	Additive	n/a	9.0 – 11.0	3.93 – 4.73	n/a	n/a
16 ⁵⁶	2017	Fraction	n/a	27.0 – 42.0	3.48 – 3.50	4.13 – 4.30	8.0 – 13.0
17 ⁵⁷	2018	Oil Source	9.4 – 17.2	20.8 – 29.8	3.49 – 3.50	4.42 – 4.61	7.0 – 9.5
18 ⁵⁸	2018	Additive	n/a	n/a	3.44 – 3.47	4.45 – 4.46	n/a
19 ¹⁸	2019	Additive	6.1 – 7.1	10.2 – 13.3	3.26 – 3.96	4.70 – 5.35	4.0 – 5.0
20 ⁶⁰	2021	Oil Source	n/a	23.7 – 33.8	3.49 – 3.53	n/a	n/a
21 ⁶¹	2021	Additive	20.6 – 21.5	32.6 – 36.2	3.55 – 3.62	4.44 – 4.52	10.3 – 11.2

222

223 The XRD data of asphaltenes from various geological sources, and often analyzed under
224 different experimental conditions, exhibit broadly similar dimensions (Table 1). However, there are
225 discernible differences in the stack diameters, stack thicknesses, interlayer spacing and aliphatic
226 distances. These dimensions correlate with the primary asphaltene particles, which are sometimes
227 denoted as ‘crystallites’ in the solid state, or ‘micelles’ in solution. It is perhaps noteworthy that most
228 XRD experiments on asphaltenes have been conducted in the solid state, however one report studied
229 them in concentrated solutions.⁵² This is undoubtedly because the amorphous background arising from
230 any solvent can often dominate the scattering contribution from asphaltene. On the other hand, the
231 degree of solvent swelling of the primary aggregates reported for various asphaltene dispersions cannot
232 be precisely assessed by a solid state approach, therefore XRD data collected from asphaltene powders
233 should be considered a *post mortem* result. Nevertheless, there is generally good agreement between
234 the structural parameters calculated from SAXS/SANS analyses of primary asphaltene aggregates in
235 solution and those obtained by solid state XRD (*vide infra*, Tables 1 – 3). This suggests that analyzing
236 the stacking of asphaltene molecules after removal of the solvent can provide valuable insights into
237 structures that were present in solvent.

238 Given the broad range of asphaltene sources, the various preparation conditions used and
239 differing instrument set-ups, quantitative comparison between various studies should only be attempted

240 with appropriate caution. Nevertheless, it is clear that (i) the source (and hence chemical composition)
241 of a given asphaltene, (ii) the method by which it was processed, (iii) the conditions of analysis
242 (primarily temperature) and (iv) the presence of any additives can each affect the asphaltene aggregate
243 morphology observed in the solid state (see Table 1 for a summary of the data obtained with each of
244 the listed variables).

245 Yen and co-workers analyzed asphaltenes that had been isolated and processed from various
246 crude oils using identical protocols.³⁹ Such asphaltenes differed significantly in the fraction of aromatic
247 carbon atoms within the material (aromaticity, f_a), which ranged from 0.14 – 0.59, but their structural
248 morphology remained relatively constant (Table 1, entry 1). In particular, all d_m values fell in the range
249 of 3.55 – 3.60 Å, as expected for amorphous carbon materials. Similarly, d_r and L_c values were also
250 relatively invariant (e.g. $L_c = 17 – 20$ Å), suggesting similar numbers of asphaltene molecules per stack
251 in all cases. However, the mean stack diameter (L_a) varied more significantly (10 – 16 Å), and with little
252 correlation to asphaltene aromaticity. This early study suggests that, despite the differing chemical
253 compositions of these asphaltenes, their primary aggregate morphology was almost constant. Later, the
254 Yen group applied the same XRD techniques to coal-derived asphaltenes processed using five different
255 protocols.⁴³ Core diameters ($L_a = 8.0 – 10.3$ Å) and mean stack thicknesses ($L_c = 10 – 14$ Å) were
256 significantly lower than those in their earlier study,³⁹ indicating that morphological differences can arise
257 from the asphaltene origin (i.e. whether extracted from solid coal or crude oil).

258 Christopher et al. used XRD to study the structure of asphaltenes derived from bitumen
259 processed at three different refineries.⁴⁴ Two samples exhibited remarkably different L_a values (ca. 12
260 and 18 Å), while all other parameters were relatively invariant (Table 1, entry 3). Moreover, the 002
261 peak was absent in the third sample, suggesting little correlation between aromatic groups. The authors
262 proposed that this indicated smaller, randomly oriented aromatic domains. ¹H and ¹³C NMR
263 spectroscopy studies indicated on average fewer aromatic rings per sheet within the third sample, which
264 would rationalize the disordered structure observed by XRD.

265 Shirokoff et al. studied four asphaltenes of varying heteroatom (i.e. N, S and O) content and
266 aromatic character.⁴⁵ Despite these chemical differences, similar structural parameters were calculated

267 for each asphaltene (Table 1, entry 4). Moreover, most of these values were in good agreement with
268 those reported in earlier studies. The exception was the mean stack thickness L_c , which was determined
269 to be 22.7 – 24.7 Å, larger than measured by Yen and co-workers.^{39, 43} In a more recent study into the
270 influence of heteroatoms, Hemmati-Sarapardeh et al. conducted XRD analysis of asphaltenes obtained
271 from three different crude oils.⁵⁷ Mean aromatic and aliphatic distances remained relatively constant,
272 but the L_a and L_c values varied significantly depending on the asphaltene origin (9.4 – 17.2 Å and 20.8
273 – 29.8 Å, respectively). The asphaltene containing the fewest heteroatoms comprised stacks of fewer
274 molecules (i.e. lower M_e). This observation contradicted the findings of Shirokoff et al., suggesting
275 heteroatom-based interactions in asphaltene stacking can affect the extent of π - π^* interactions between
276 aromatic rings and should not be overlooked. Very recently, Hemmati-Sarapardeh et al. studied three
277 crude oils by XRD to assess their ‘thermal maturity’, which is a geochemical parameter that quantifies
278 the degree of chemical aging that takes place over time.⁶⁰ This technique indicated that greater aromatic
279 character, an increase in intermolecular spacing (d_m) and a reduction in L_c serve as useful markers for
280 enhanced crude oil maturity. Moreover, such XRD data was in good agreement with Raman spectra
281 and conventional thermal maturity analytical methods.

282 Some studies have examined the effect of fractionation on structural parameters of the resultant
283 asphaltenes. For example, Bansal et al. observed significant differences in the initial mean diameter of
284 aromatic cores of two sources of asphaltenes containing differing heteroatom content and aromaticity
285 (see entry 6 in Table 1).⁴⁷ These asphaltenes were fractionated by column chromatography using
286 solvents of varying polarity. In general, employing more polar solvents led to thicker stacks within the
287 precipitated asphaltene (L_c). ¹H NMR and elemental microanalysis indicated that asphaltene fractions
288 isolated using polar solvents contained less-substituted aromatic ring structures, enabling more efficient
289 packing and thicker stacks. Furthermore, higher oxygen contents were detected in the more polar
290 fractions, suggesting more carbonyl groups that could form H-bonding interactions that favor stacking.

291 Andersen et al. also used solvent-based fractionation to analyze asphaltene precipitates isolated
292 from various heptane-toluene mixtures (this binary solvent mixture is often denoted as ‘heptol’).⁴⁹
293 Asphaltenes precipitated from four different crude oils in pure *n*-heptane exhibited significantly

294 different L_a and L_c values (Table 1, entry 8). However, increasing the proportion of toluene in the heptol
295 precipitation solvent produced no systematic trends with regard to the asphaltene morphology. The
296 authors critically discussed the use of XRD for microstructural analysis of asphaltenes, in particular the
297 experimental uncertainties associated with baseline and peak fitting during XRD data analysis. Errors
298 can be incurred depending on the individual operator and software program, so developing a
299 standardized protocol is essential for comparison between datasets. For example, they found that much
300 better fits could be achieved using a Gaussian line shape rather than a Lorentzian line shape, but the
301 former method required more manual refinement that could introduce greater operator bias. In addition,
302 aromaticity fractions (f_a) estimated by XRD analysis were always significantly lower than estimated by
303 ^1H NMR spectroscopy and it was suggested that only a fraction of the aromatic rings actually participate
304 in the formation of asphaltene stacks.

305 Shirokoff et al. published a detailed XRD study of asphaltenes originating from various
306 sources,⁵⁹ using several peak functions such as Pearson VII, Pseudo-Voigt and Generalized Fermi.
307 Good agreement was obtained for most fittings. Generally speaking, d_m values were approximately 1 Å
308 larger, and L_a and L_c values were significantly smaller relative to all other studies summarized in Table
309 1. This observation may be related to the accelerated aging to which asphaltenes were subjected prior
310 to their analysis. The authors suggested might lead to significant chemical changes, although no
311 chemical analysis was undertaken to examine this hypothesis.

312 Kananpanah et al. studied the effect of temperature used in a thermal ‘de-asphaltene’ process,
313 whereby heat is used to induce asphaltene aggregation and fractionation within crude oil prior to
314 filtration.⁵⁴ Increasing the de-asphaltene temperature from 60 to 120 °C increased the yield and led to
315 thicker stacks with up to 15 molecules per stack (see entry 14 in Table 1). However, raising this
316 temperature above 120 °C led to reduced mean stack thickness and a lower yield. Asphaltenes
317 comprising lower aromatic contents tended to form thicker primary particles, which somewhat
318 contradicts the findings of Christopher et al.⁴⁴ In a follow-up study, the authors compared products of
319 thermal ‘de-asphaltene’ to solvent-based precipitation in *n*-heptane and a ‘thermal-toluene’ method,
320 whereby asphaltenes retained on filters following thermal precipitation were extracted in toluene,

321 followed by evaporation.⁵⁶ Larger stacks were obtained from the solvent-based method than the two
322 thermal methods, which was attributed to the longer timescale of *n*-heptane addition enabling more
323 molecules to stack together. The authors' analysis also revealed a correlation between d_r and M_e , with
324 closer aliphatic packing being observed in stacks containing more asphaltene molecules. This suggests
325 that more closely associated alkyl chains at the periphery may help promote molecular stacking.

326 Several studies have focused on the effect of thermal treatment of asphaltenes on their structure,
327 using experiments designed to represent aging or refinery processes. Siddiqui et al. studied the effect of
328 thermal annealing on the chemistry and morphology of Ras Tanura (RT) and Kuwait (KW)
329 asphaltenes.⁴⁶ A rolling thin film oven was employed for short-term aging studies, while a pressurized
330 vessel was used for long-term aging (temperatures and pressures not provided). For the RT asphaltene,
331 the mean aromatic and aliphatic distances (d_m , d_r) decreased over time, concomitant with an increase
332 from 5 to 7 molecules per stack. These changes were confined to short-term aging: no further structural
333 changes were observed during long-term aging. In contrast, the KW asphaltene structure continued to
334 evolve during long-term aging. The different aging behavior observed for KW asphaltenes was
335 attributed to the higher heteroatom content and greater aromatic character; such differences are expected
336 to provide additional reaction pathways for oxidative aging, which lead to looser molecular stacking.

337 Tanaka et al. reported *in situ* studies of the effect of temperature on morphology using
338 asphaltene isolated from three different sources.⁴⁸ At 30 °C, all three asphaltenes exhibited identical d_m
339 values and similar L_c (Table 1, entry 7), the latter of which significantly decreased in each case upon
340 heating (from 25.2 Å at 30 °C to as low as 13.7 Å at 300 °C). Despite the 50% reduction in the mean
341 number of molecules per stack, the primary asphaltene particles still persisted at elevated temperatures
342 relevant to end-user applications. Furthermore, these data suggest that the environmental conditions
343 have a more significant influence than the chemical composition of the asphaltene on the nanoaggregate
344 dimensions.

345 Trejo et al. compared asphaltenes extracted from a crude oil that had undergone catalytic
346 hydrotreatment under various conditions.⁵⁰ The process involved flowing crude oil in a diluent over a
347 particulate catalyst at variable pressure, temperature, and flow rate. Asphaltenes were then isolated from

348 the treated crude oil and subsequently analyzed by XRD. The mean number of molecules within isolated
349 asphaltene stacks was reduced from 20.7 from untreated crude oil to 8 – 11 after catalytic
350 hydrotreatment, regardless of the conditions employed (see entry 9 in Table 1). In all cases, harsher
351 reaction conditions led to small but significant reductions in d_m . ^{13}C NMR analysis indicated that more
352 severe conditions led to shorter aliphatic tails and also reduced the mean degree of ring substitution.
353 Such changes should facilitate more efficient packing between asphaltene molecules, which was
354 consistent with the observed reduction in the mean interlayer spacing towards the limiting value for
355 graphite (3.34 Å).³⁹ However, the authors emphasized that experimental evidence linking the isolated
356 solid-state asphaltene structure to dispersions in crude oil is lacking.

357 Al-Humaidan et al. investigated how thermal cracking of vacuum residues impacted the
358 chemical structure and morphology of asphaltenes.⁵³ Three different vacuum residues were subjected
359 to nine different reaction conditions at 400, 415, or 430 °C for 30, 50, or 60 min prior to asphaltene
360 extraction. Contrary to the data reported by Trejo et al.,⁵⁰ d_m and d_r both increased as harsher cracking
361 reaction conditions were employed (Table 1, entry 13). However, the most significant morphological
362 change was observed in L_c , which was reduced from 13.3 Å (untreated) to as low as 7.8 Å when
363 employing the most severe conditions. This observation could be explained by more aliphatic groups
364 cleaving, resulting in a higher aromatic fraction (increasing from 0.14 to > 0.4 as measured by XRD).

365 XRD has also been used to study the effect of additives on the structure of primary asphaltene
366 aggregates. Mousavi et al. investigated the effect of adding a hexadecamide binder to an asphalt-binder
367 mixture (comprising asphaltene and other components of crude oil) using a combination of XRD and
368 density functional theory (DFT).⁵⁵ XRD analysis showed that the additive significantly reduced both
369 the interlayer stacking and the mean stack thickness of the asphalt binder. DFT calculations indicated
370 that the amide group should form hydrogen bonds with the polar groups in asphaltene, leading to weaker
371 intermolecular quadrupolar interactions and influencing the nanoaggregate dimensions. Moreover, the
372 n-hexadecyl chains interacted with the pendent aliphatic groups on asphaltene molecules via van der
373 Waals' forces. Afra et al. investigated the effect of adding a mixture of three phenolic amphiphiles
374 (anacardic acid, cardanol and cardol, denoted 'ACC') on asphaltene aggregation.⁵⁸ These 'green'

375 additives were believed to interact with asphaltenes via hydrogen bonding, stacking, and acid-base
376 interactions. Although the presence of ACC reduced the crude oil viscosity and significantly delayed
377 the onset of asphaltene precipitation, XRD studies indicated only minimal changes at the molecular
378 level (d_m increased by $< 0.05 \text{ \AA}$). Meanwhile the measured aromatic fraction decreased, suggested
379 partial solubilization of asphaltenes. These results were verified by peak-fitting protocols employing
380 either Gaussian or Lorentzian functions, and potential limitations of this technique were highlighted.

381 Alhreez et al. used XRD to investigate the effect of p-dodecylbenzenesulfonic acid (DBSA,
382 Figure 7) on precipitated asphaltene morphology.^{18, 62} The d_m values increased significantly from 3.26
383 to 3.65 \AA in the presence of this additive, while d_r also increased from 4.70 to 5.25 \AA (Table 1, entry
384 19). Moreover, DBSA addition also reduced the average molecules per stack from 5 to 4, and decreased
385 the mean stack diameter. These results indicated the formation of looser asphaltene stacks in the
386 presence of this additive. Asphaltene precipitation could also be controlled by delivering the DBSA in
387 the form of a microemulsion, which resulted in larger changes in morphology compared to simple
388 addition of this stabilizer.¹⁸ More specifically, d_m increased to 3.96 \AA and d_r increased up to 5.35 \AA ,
389 with further modest reductions in L_c and L_a . Indeed, the overall aromatic fraction of the asphaltene was
390 lowered from 0.35 to as low as 0.22 for both samples prepared in the presence of DBSA. Based on these
391 data, the authors proposed that H-bonding and π - π^* interactions between the DBSA surfactant and
392 asphaltene led to steric interference that prevented further π - π^* stacking into larger asphaltene
393 aggregates. The authors also suggested that the sulfonate groups on the dispersant could potentially
394 react with asphaltenes via electrophilic addition.

395 Wang et al. designed an amphiphilic copolymer to disperse asphaltene aggregates in crude oil.⁶¹
396 This copolymer comprised cationic surfactant moieties to impart surface activity, an amphiphilic side
397 chain containing both polyether and *n*-alkyl segments to adjust the hydrophilic-lipophilic balance, and
398 an aromatic/aliphatic tertiary amine to interact with the asphaltene. Precipitated asphaltenes were
399 vigorously mixed with excess copolymer, resulting in an increase in d_m and a reduction in L_c relative to
400 the control experiment performed with non-interacting polyacrylamide. The authors concluded that the

401 rich functionality presented by the amphiphilic copolymer enabled it to form non-covalent bonds with
402 asphaltenes, thus disrupting intermolecular interactions and effectively reducing the crude oil viscosity.

403 Each of the above articles involved XRD studies of asphaltenes in the solid state after their
404 isolation via precipitation. However, Hoepfner and Fogler demonstrated that X-ray scattering analysis
405 can be performed on 5% (v/v) asphaltene dispersions in toluene, THF, or 1-methylnaphthalene (see entry
406 11 in Table 1).⁵² After appropriate solvent background subtraction, interlayer stacking distances ($d_m =$
407 $3.45 - 3.52 \text{ \AA}$) were found to be closely related to those previously reported for asphaltenes in the solid
408 state (Table 1, entries 1 – 10). However, an additional shoulder between the γ -band and 002 peak was
409 observed. This “002” peak was attributed to the packing of disordered asphaltene cores over longer
410 length scales ($3.8 - 4.1 \text{ \AA}$). The d_r parameter varied with the dispersing solvent, suggesting that the
411 peripheral aliphatic chains swelled differently in different solvents.

412 **SAXS and SANS**

413 SAS techniques have been employed on numerous occasions to study asphaltene ‘drop-out’. Both
414 techniques require sufficient contrast between the asphaltene molecules and their surrounding media
415 for meaningful data to be collected. SAXS relies on the difference in *scattering length density* ($\Delta\xi$),
416 which is related to the electron density difference between the asphaltene molecules and the solvent
417 medium in which they are dispersed. The high density of the polyaromatic fused ring structure of
418 asphaltene molecules usually provides sufficient electron density contrast relative to the lower density,
419 aliphatic-rich solvent (including the maltene fractions of crude oil). However, in the literature
420 asphaltenes are usually isolated from crude oil in order to prepare model systems of known
421 compositions (and also to ensure the removal of other scattering entities such as crystalline waxes and
422 minerals).^{49, 63} Sample preparation typically involves the selective precipitation of asphaltenes from
423 crude oil using a suitable aliphatic non-solvent, followed by washing with the same non-solvent (e.g.
424 by Soxhlet extraction). In contrast to XRD analysis, dry asphaltene fractions are redispersed in either
425 an organic solvent or a solvent mixture (most commonly heptol). In addition to simplifying the
426 background subtraction and data fitting procedures, using a model hydrocarbon solvent enhances the

427 electron density contrast between the heteroatom-rich asphaltene cores and the continuous phase, while
428 simultaneously reducing the $\Delta\xi$ of aliphatic chains.

429 Unlike X-ray scattering, neutron scattering depends on differences in atomic nuclei rather than
430 electrons, therefore contrast in nuclear scattering length density (which is atomic isotope-dependent) is
431 required for strong scattering. To achieve this in the case of asphaltene dispersions, the solvent or
432 solvent mixture should be partially or fully deuterated in order to increase contrast relative to the
433 hydrogenous asphaltene component. Some research groups have conducted SANS studies on crude oil
434 mixtures, but the most common practice is to isolate the asphaltenes from crude oil via precipitation,
435 before redispersing them in deuterated solvents such as d_8 -toluene and/or d_{16} -heptane. The main
436 disadvantages of SANS are (i) the lower maximum flux achievable at state-of-the-art neutron sources
437 (relative to synchrotron X-rays) and (ii) the need for expensive deuterated solvents (which may not
438 capture the complex behavior exhibited by crude oil). In practice, this means that data is acquired more
439 quickly using SAXS, which hence offers greater temporal resolution for monitoring dynamic processes.
440 On the other hand, higher contrast can be achieved with SANS compared to SAXS. Owing to the
441 neutron scattering length density contrast between the aromatic and aliphatic regions of asphaltenes it
442 is possible to determine more fine structure, for example dimensions of the core and shell of primary
443 aggregates.^{64, 65}

444 In principle, SAXS and SANS can provide the same morphological and structural data. The ‘small
445 angle’ formalism typically refers to a scattering angle, 2θ , of 0.1 to 10° for a radiation wavelength of
446 about 1 \AA , which translates into real-space length scales of approximately 1 to 100 nm . Thus, both
447 techniques enable the analysis of most aspects of highly hierarchical structures such as asphaltenes on
448 multiple length scales, from nanoaggregate size and shape to cluster size and fractal dimension.
449 However, Bonse-Hart camera or modern instruments with the sample-to-detector distance of tens of
450 meters enable data to be collected at $2\theta < 0.1^\circ$. These techniques, termed ultra-small angle X-ray or
451 neutron scattering (USAXS or USANS), expand the range of accessible real space up to $5\text{-}10 \text{ }\mu\text{m}$, which
452 includes macroscopic asphaltene precipitates.

453 Scattering data collected from SAXS and SANS experiments require significant data reduction and
454 processing and the application of an appropriate scattering model to obtain meaningful real-space
455 information. This is often considered a disadvantage of such techniques, since the same data can
456 sometimes be satisfactorily fitted using different scattering models. Typically, scattering patterns for
457 asphaltene dispersions (Figure 4) are presented as double logarithmic plots of scattered intensity (after
458 background subtraction and normalization) against modulus of scattering vector, q , which is calculated
459 from

$$460 \quad q = \frac{4\pi}{\lambda} \sin \theta \quad (1)$$

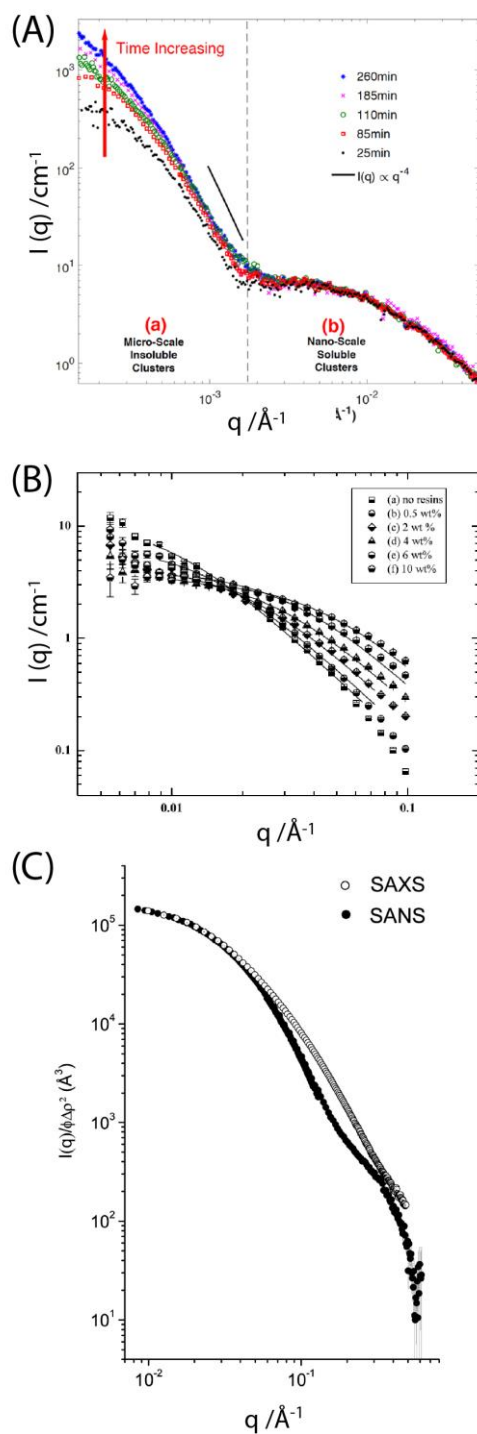
461 where θ is half of the scattering angle and λ is the radiation wavelength.

462

463

464

465



466

467 **Figure 4.** Literature examples of scattering data obtained for asphaltene samples: (A) *in situ* USAXS
 468 patterns collected during asphaltene precipitation induced by addition of *n*-heptane to a dispersion in
 469 toluene;⁶⁶ (B) SANS analysis of asphaltenes in the presence of 0-10% resin by mass;¹⁷ (C) comparison
 470 of SAXS and SANS patterns recorded for the same asphaltene dispersion in toluene and *d*₈-toluene,
 471 respectively.⁶⁴ The additional oscillations observed in the SANS data result from the fine structure

472 arising from differing neutron scattering length densities. In some cases data fits according to scattering
473 models are included (see main text for further discussion).

474

475 In general, scattered intensity is a product of two terms - the form factor, $P(\vec{q})$, and the structure
476 factor, $S(\vec{q})$. The form factor describes the size, shape, and polydispersity of particles, while the
477 structure factor is related to the arrangement of scattering particles in space, from which the mean
478 distance between the particles and the degree of inter-particle structural order can be assessed. Structure
479 factor contributions are more prevalent at higher concentrations, particularly for charged particles in
480 polar media (e.g. water). In contrast, structure factor scattering from asphaltenes in non-polar media
481 such as crude oil, model solvents or solvent mixtures tends to be insignificant. According to Barré et
482 al., no structure factor should be observed within scattering patterns recorded for dilute asphaltene
483 dispersions (i.e., below 2% concentration).⁶⁷ For colloidal dispersions producing isotropic scattering
484 patterns, the scattered intensity is described by a scalar function, $I(q)$, expressed as

$$485 \quad I(q) = \varphi(1 - \varphi)\Delta\xi^2 S(q)P(q) \quad (2)$$

486 where $P(q)$ and $S(q)$ are scalar forms of the form factor and the structure factor, respectively, φ is the
487 particle concentration and $\Delta\xi^2$ is the square of the scattering length density contrast between the
488 asphaltene molecules/particles and the surrounding medium. $S(q)$ in equation (2) can be taken to be
489 unity for sufficiently dilute dispersions of asphaltene in non-polar media.

490 Various analytical methods can be applied to analyze scattering from asphaltene dispersions,
491 and one of the most commonly adopted approaches is derived from Guinier's law, which relates
492 scattered intensity to the radius of gyration (R_g) of particles (more specifically, the largest hierarchical
493 object formed in the studied system).⁶⁸

$$494 \quad I(q) = I(0)e^{-q^2 \frac{R_g^2}{3}} \quad (3)$$

495 where $I(0)$ is scattered intensity at $q = 0$, obtained by extrapolating the fitted curve to $q = 0$ (e.g. Figure
496 5A). For a dilute solution of relatively homogeneous particles this term is expressed as $I(0) = \varphi(1 -$

497 $\varphi)\Delta\xi^2V_{\text{part}}$ where V_{part} is volume of an averaged scatterer (particle) and the term related to the particle
498 volume concentration could be simplified for small concentrations as $\varphi(1 - \varphi) \approx \varphi$. From a plot of
499 $\log I(q)$ vs q^2 , the R_g can be derived from the low q gradient using equation (3). Taking that the particles
500 are spherical objects the R_g can then be related to the particle radius, R , through the relationship:

501
$$R_g = \sqrt{\frac{3}{5}} R \quad (4)$$

502 However, a spherical morphology cannot always be assumed for asphaltene particles, and numerous
503 studies have evaluated shape-dependent small-angle scattering (SAS) models.^{64, 69, 70} The Guinier
504 approximation only applies if $qR_g \ll 1$. The Zimm approximation is an alternative data treatment
505 method that holds for higher q values (i.e. for qR_g up to 3):⁷¹

506
$$\frac{1}{I(q)} = \frac{1}{I(0)} \left(1 + q^2 \frac{R_g^2}{3} \right) \quad (5)$$

507 where all parameters have a similar meaning as in equation (3) (Figure 5). It has been argued that the
508 above treatments cannot be applied to scattering data from asphaltenes owing to their highly
509 polydisperse nature.^{70, 72} Alternative approaches including Beaucage (also known as unified fit),⁷³ and
510 Schultz^{70, 72, 74, 75} parametrizations have also been applied to obtain mean dimensions and morphologies
511 of asphaltene aggregates at different hierarchical levels. If particles have isotropic shape, then its mean
512 size can be calculated from the R_g value [equation (4)]. However, the morphology of asphaltene
513 aggregates, including primary particles, has been a somewhat controversial topic.⁵ Several research
514 groups have compared numerous models,^{64, 70, 73, 76-78} with satisfactory data fits requiring various
515 assumptions to be made regarding the particle morphology. Sirota has demonstrated that the scattering
516 from asphaltene dispersions may be rationalized in terms of a binary mixture of phase-separated
517 liquids.¹⁶ In this case, the Guinier region can be described by a Lorentzian line shape arising from
518 concentration fluctuations.

519 Information on the molecular weight, $\overline{M_w}$, of asphaltene nanoaggregates can be estimated based
520 on the intensity obtained from $I(0)$ using the following relationship:

521
$$\overline{M}_w = \frac{I(0)N_A\rho}{\varphi(1-\varphi)\Delta\xi^2} \quad (6)$$

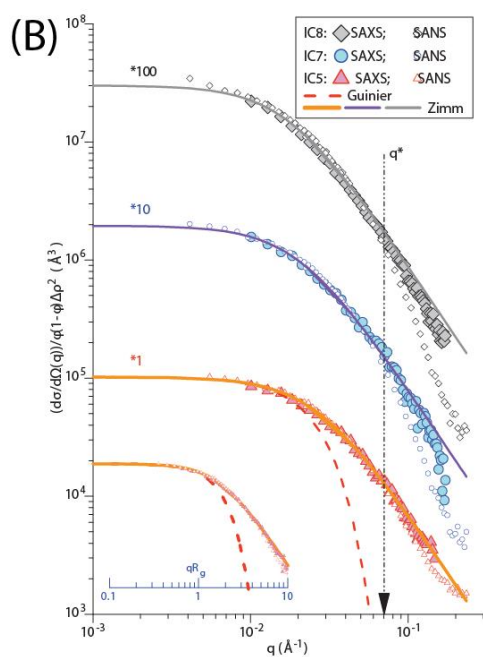
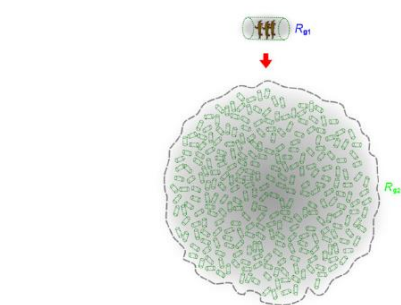
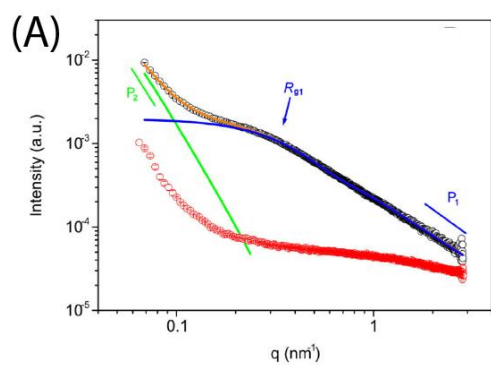
522 where it is assumed that the nanoaggregate volume is expressed as $V_{\text{part}} = \frac{\overline{M}_w}{N_A\rho}$, N_A is Avogadro's
523 number, and ρ is the mass density of asphaltene.

524

525

526

527



528

529 **Figure 5.** (A) SAXS Zimm plot fit (blue) to calculate the radius of gyration (R_{g1}) and regions P_1 and P_2
 530 where power laws are determined to obtain fractal dimensions of soluble (higher q) and insoluble (lower
 531 q) asphaltene fractions (assigned as 1 and 2, respectively).⁷⁹ The red pattern represents the background,
 532 which comprises the crude oil maltenes from which the asphaltenes were separated. (B) Comparison of
 533 Guinier and Zimm models fit (dashed and solid curves) to SAXS and SANS data (open and solid

534 symbols, respectively) recorded for an asphaltene solution in toluene; the Zimm plot clearly offers a
535 better fit to both SAXS and SANS data at higher q .⁶⁵

536

537 The aggregate structure of asphaltene is highly hierarchical.^{18,11} Although the Guinier and
538 Zimm approximations provide useful information regarding the size and morphology of the primary
539 units (i.e. stacks of asphaltene molecules), higher order structures require additional data analysis. The
540 latter structures are best described as mass fractals, which have a characteristic fractal dimension, d_f .
541 This parameter can be calculated by plotting M_w vs R_g values obtained by SAS analyses, from a series
542 of asphaltene dispersions measured under various conditions. The fractal dimension can be calculated
543 from the gradient (Figure 6A) using the following relationship:

$$544 \quad M_w \propto R_g^{d_f} \quad (7)$$

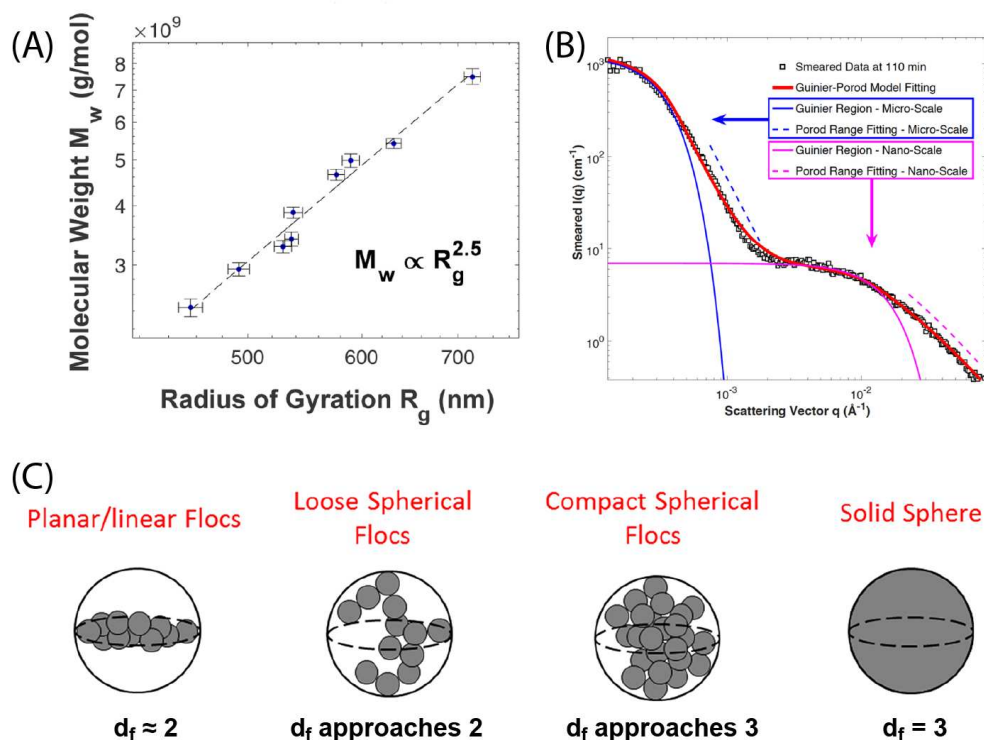
545 An alternative method to analyze fractality is to calculate the gradient, P , of the scattered
546 intensity in the Porod's region:

$$547 \quad I(q) \propto q^{-P} \quad (8)$$

548 A few Porod's regions could be observed for the hierarchical structure of asphaltenes. In this
549 case P can be determined from different (high and low) q ranges to calculate the fractality of the
550 nanoaggregates and larger clusters, respectively (Figure 6B). In general, if $1 < P < 3$, its numerical value
551 is directly related to the fractal dimension (d_f) mainly associated with mass fractals of the asphaltene
552 aggregate, with higher P values indicating denser, less solvated structures. When $4 > P > 3$, this indicates
553 a formation of dense aggregates with a relatively homogeneous internal structures but with a significant
554 interfacial roughness associated with surface fractals. In this case, the power law exponent in Eq (8) is
555 related to the fractal structure dimensions as $P = 2d_f - d_s$, where d_s is the surface fractal dimensions and
556 d_f is about 3. As P tends to 4, this corresponds to smooth sharp interfaces between asphaltene particles
557 and the surrounding medium⁸⁰ when $d_s = 2$ and $d_f = 3$.

558 However, such approaches for estimating fractal dimensions have been criticized by Gawrys et
 559 al.⁷⁶ These researchers suggest that power law analysis is affected by overlap with different scattering
 560 regions, while the M_w vs R_g approach implicitly assumes that all samples possess the same fractal
 561 dimension. Alternative models have been applied to asphaltene SAS data, where a fractal structure
 562 factor is included within the SAS model alongside particle size etc.⁸¹

563



564

565

566 **Figure 6.** Analytical methods applied to scattering data to calculate the fractal dimension of asphaltene
 567 aggregates taken from the literature.⁶⁶ (A) the power law relationship between molecular weight, M_w ,
 568 and radius of gyration, R_g , and (B) by fitting power laws in the Porod region of data recorded over
 569 various q ranges to obtain information regarding the soluble (high q) and insoluble (low q) asphaltene
 570 fractions (see pink and blue dashed lines, respectively). (C) Schematic representation of the proposed
 571 evolution of asphaltene structure as the fractal dimension (d_f) increases.⁸²

572

Table 2. Summary of literature reports of the morphological characterization of asphaltenes determined by SAXS and USAXS analysis in chronological order

Entry & ref	Geological Origin(s)	SAS model(s) for R_g calculation	Variables studied	$R_g / \text{\AA}$	$M_w / \text{kg mol}^{-1}$	d_f
1 ⁸³	Lagunillas, Santa Maria, Tia Juana, Bartlesville, Bachaquero, Rhodes	Guinier (sol)	Temperature	34 – 38	N/A	N/A
	Concentration		34 – 55			
	Oil source		31 – 69			
	Solvent		33 – 35			
2 ⁸⁴	Boscan, Kuwait, Ragusa, Baxterville, Lagunillas	Porod and Guinier	Concentration	33 – 40	N/A	N/A
	Solvent		34 – 38			
3 ⁸⁵	Grenada, Permatang, Safaniya	Thin disk	Oil source	N/A	N/A	1.59 – 1.69
4 ⁷⁴	Duri, Ratawi, Oriente, Merey	Schultz distribution of spheres	Oil source	34 – 51	N/A	N/A
			Concentration	~29 ¹ – 34		
5 ⁸⁶	N/A	Guinier	Additive	37 – 75	N/A	N/A
6 ⁸⁷	Athabasca	Guinier	None	33	N/A	N/A
7 ⁸⁸	Safaniya	N/A	Solvent	N/A	N/A	3.37 – 4.00
8 ⁸⁹	Safaniya	Zimm	Fraction	33 – 252	24 – 1560	1.99 – 2.06
9 ⁹⁰	N/A	Zimm	Oil Source	55 – 66	75 – 115	N/A
10 ⁹¹	South East Mexico	Guinier	Fraction	190 – 255	N/A	1.57 – 1.61
			Solvent	192 – 255		1.57 – 1.61 ¹
			Kinetics	163 – 255		1.61 – 1.72
11 ^{92*}	Safaniya	Guinier/Zimm	Temperature	35	N/A	2.05
12 ^{75*}	Ratawi, Oriente, Merey, Duri	Schultz	Concentration	~33 – 36 ¹	N/A	N/A
			Oil source	~30 – 44 ¹		
13 ⁶⁷	Saudi Arabia	Zimm	Fraction	63 – 160	198 – 666	2.10 – 2.20
14 ⁶⁵	Safaniya	Zimm	Solvent	66 – 106	N/A	2.10 – 2.20
15 ⁹³	Siberia, Tatarstan, Mongolia	Guinier	Source	22 – 24	N/A	N/A
			Solvent	23 – 24		
16 ^{64*}	Safaniya	Zimm	Model	71	16	N/A
17 ⁶³	Safaniya	Zimm	Fraction	25 – 58	20 – 148	1.70 – 3.00
			Temperature	40 – 58	88 – 148	
18 ⁹⁴	Safaniya	Zimm	Temperature	33 – 41	47 – 69	1.50
19 ^{52*}	N/A	Zimm	Concentration	~40 – 80 ¹	~18 – 50 ¹	1.70

			Solvent	~20 – 50 ¹	~20 – 100 ¹	
			Oil source	~20 – 55 ¹	~20 – 50 ¹	
20 ⁹⁵	Canada	Zimm	Concentration	34 – 55	55 – 84	1.70
			Solvent	34 – 47	40 – 55	
21 ⁷⁹	Brazil	Multi-level unified model (Igor)	Concentration	35 – 46		2.20 – 2.70
			Oil source	27 – 46	N/A	1.80 – 3.20
			Solvent	24 – 31		2.20 – 3.20
			Additive	26 – 46		1.50 – 2.40
22 ⁶⁶	Athabasca	Guinier	Solvent	~90 – 190 ¹	~160 – 450 ¹	1.40 – 1.75
			Kinetics	4560 – 7160	~2.4 x 10 ⁶ – 7.4 x 10 ⁶ ¹	3.60 – 4.00
			Fraction	95 – 4560	~450 – 7.4 x 10 ⁶ ¹	1.60 – 2.50
23 ⁹⁶	N/A	Other	Source	~26 – 34 ¹	N/A	N/A
			Kinetics	~26 – 58 ¹		
24 ⁹⁷	USA	Guinier	Additive	56 – 150	N/A	2.35 – 2.96
25 ⁹⁸	N/A	Guinier	Kinetics	~83 – 95 ¹		2.30 – 2.80
			Additive	~77 – 100 ¹	N/A	2.40 – 3.30
			Solvent	~24 – 80 ¹		N/A

* = SANS also conducted in these studies (see Table 3), ¹numbers estimated from graphical plots. N/A = data not available

Table 3. Summary of literature reports of the morphological characterization of asphaltenes determined by SANS or USANS analysis in chronological order

Entry & Ref	Geological Origin(s)	SAS model(s) for R_g calculation	Variables studied	R_g (or other aggregate dimension)/Å	M_w / kg mol ⁻¹	d_f
1 ⁶⁹	Safaniya	Spheroid/disk	Fraction	$D_{\text{disk}} = 130 - 850$	16 - 89	N/A
			Concentration	$D_{\text{disk}} = 115 - 150$	29 - 50	
			Solvent	$D_{\text{disk}} = 90 - 180$	29 - 77	
			Oil source	$D_{\text{disk}} = 130 - 160$	33 - 59	
2 ⁷²	Ratawi	Schultz	Solvent	30 - 32	N/A	N/A
			Concentration	31 - 32		
3 ⁷⁰	Arab Heavy	Cylinder and Schultz	Temperature	50 - 54	N/A	N/A
			Model	26 - 54		
4 ⁸¹	Ratawi	N/A	Concentration	N/A	N/A	1.80 - 3.00
			Temperature	12 - 47 ¹	N/A	1.05
5 ⁹⁹	Maya	Guinier	Solvent	61 - 199	112 - 1200	N/A
			Oil source	144 - 199	569 - 1200	2.05 - 2.20
7 ^{88*}	Safaniya	N/A	Solvent	N/A	N/A	3.57
			Concentration	30 - 52	21 - 55	~2.00
8 ⁷⁸	Safaniya	Guinier & Zimm	Temperature	50 - 80	50 - 130	N/A
			Model	43 - 49	53 - 54	N/A
			Oil source	$R_{\text{sphere}} = 31 - 42$	N/A	N/A
9 ¹⁰¹	Maya, Khafji, Iranian light	Guinier and fractal	Solvent	$R_{\text{sphere}} = 33 - 50$	N/A	N/A
			Temperature	$R_{\text{sphere}} = 23 - 46$	2.42-2.72	
			Additive	128	N/A	N/A
10 ¹⁷	B6, Hondo, Safaniya, Canadon Seco	Guinier	Solvent	$\text{Correlation Length} = 43 - 79$	N/A	N/A
			Oil source	$\text{Correlation Length} = 40 - 57$		
			Additive	$\text{Correlation Length} = 38 - 110$		
			Solvent	$\text{Correlation Length} = 40 - 90$		
11 ¹⁰²	B6, Hondo, Safaniya, Canadon Seco	Guinier	Oil source	$\text{Correlation Length} = 30 - 200^1$	40 - 1000	1.70 - 2.10
			Fraction	$\text{Correlation Length} = 80 - 450^1$	100 - 10000	N/A
			Oil source	$\text{Correlation Length} = 26 - 65^1$	N/A	1.10 - 3.80
			Oil source	$\text{Correlation Length} = 26 - 65^1$	N/A	1.10 - 3.80

			Kinetics	<i>Correlation Length = 26 – 57</i>		1.10 – 4.10
13 ^{92*}	Safaniya	Guinier/Zimm	Temperature	35 – 65	33 – 115	N/A
14 ^{75*}	Ratawi	Guinier	Solvent	30 – 31	N/A	N/A
15 ⁷⁷	Hondo,	Numerous models	Oil source	45 – 58	N/A	2.63 – 2.76
	Canadon		Concentration	43 – 71		2.52 – 2.61
	Seco, Arab Heavy		Model	58 – 75		N/A
16 ⁷⁶	B6, Hondo,	Numerous models	Oil source	51 – 131	10 – 1000	N/A
	Arab Heavy,		Fraction	62 – 131		N/A
	Gulf Coast, Canadon Seco		Solvent	63 – 113		2.20 – 3.00
17 ^{64*}	Safaniya	Zimm sphere or cylinder	Model	$R_{\text{sphere/cylinder}} = 18 – 20$	N/A	N/A
				$R_{\text{shell}} = 10 – 14$		
			Oil source	35 – 37		
18 ⁷³	N/A	Beaucage, Zimm	Temperature	32 – 37	N/A	2.20 – 2.98
			Model	37 – 46		N/A
			Temperature	3470 – 4690		2.23 – 2.98
19 ¹⁰³	N/A	Zimm	Solvent	15 – 43	250 – 1000	1.70 – 1.98
			Kinetics	23 – 35	2000 – 5000	N/A
			Oil source	6 – 43	200 – 1000	1.23 – 1.98
			Fraction	N/A	N/A	1.69 – 2.12
20 ¹⁰⁴	Llanos, Athabasca	Broad peak model	Fraction	<i>Correlation Length = 29 – 60</i>	N/A	2.20 – 2.86
			Solvent	<i>Correlation Length = 26 – 28</i>		2.86 – 2.90
			Oil source	<i>Correlation Length = 25 – 28</i>		2.86 – 2.99
21 ¹⁰⁵	Norwegian	Guinier	Solvent	29 – 35	14 – 25	N/A
			Concentration	29 – 32	N/A	

* = SAXS also conducted in these studies (see Table 2), ¹estimated from graphical plots. N/A = data not available

573 Given that asphaltene dispersions comprise a broad range of both molecular and aggregate
574 structures, there is typically significant overlap between the Guinier and Porod regions.⁹⁸ Consequently,
575 the best practice usually involves the simultaneous application of multiple models to SAS data over a
576 broad q range (see Figure 6B). The hierarchical nature of asphaltene aggregation means that different
577 structural aspects can be analyzed by analyzing an appropriate q range. In practice, this can be achieved
578 by adjusting the sample-to-detector distance used in the instrument set-up. Typically, for q ranging from
579 0.001 to 0.5 Å⁻¹, scattering is predominantly from ‘soluble’ asphaltene nanoaggregates (i.e. < 100 nm),

580 which enables calculation of R_g , M_w , and d_f . For $q < 0.001 \text{ \AA}^{-1}$, this corresponds to scattering from larger
581 insoluble clusters, with such data requiring the use of ultra-small-angle scattering (USAS) techniques.⁶⁶
582 There are many literature reports of data fits to scattering patterns recorded for asphaltene dispersions
583 over a wide q range. Since these experiments were performed on asphaltenes obtained from a broad
584 range of sources, analyzed under various conditions and using differing instrumental set-ups,
585 quantitative comparisons between studies should be made with caution. Nevertheless, there is often
586 quite good agreement between quantitative analysis in such studies. Tables 2 and 3 summarize the
587 fitting parameters used for SAS analysis (SAXS and SANS, respectively) that enable comparison of the
588 morphology of asphaltene aggregates from various crude oil sources, processed by different reaction
589 conditions or fractionation methods, and analyzed at various temperatures, concentrations, solvents, and
590 pressure, with or without additives.

591 Dwiggin was the first to conduct SAXS analyses on crude oils in order to characterize colloidal
592 structures present.⁸³ In this pioneering study the Guinier approximation was used to calculate the R_g ,
593 which ranged from 30 to 70 \AA for 7 different crude oils. Crude oils were also analyzed at elevated
594 temperature and after dilution in mineral oil or *cis*-decahydronaphthalene. Temperature and dilution in
595 *cis*-decahydronaphthalene had relatively minor impact on dimensions, but dilution in mineral oil led to
596 a systematic increase in R_g . This observation was attributed to the poor solubility of asphaltene in
597 mineral oil leading to further aggregation upon dilution. The author briefly discussed the likely particle
598 morphology and alluded to the possibility of ellipsoidal asphaltene particles in addition to pseudo-
599 spherical particles.

600 Pollack and Yen compared the scattering from asphaltenes to structurally-related resin and carbon
601 black samples.⁸⁴ Asphaltenes were isolated from several crude oils and analyzed both in the solid state
602 (by Porod analysis) and as colloidal dispersions (using Guinier analysis). SAXS studies of asphaltenes
603 in the solid state enabled calculation of mean particle diameters of 300 – 400 \AA , which were smaller
604 than values obtained for resins and other amorphous carbons under the same experimental conditions.
605 For colloidal dispersions of asphaltenes, R_g was measured in the region of 33 – 40 \AA , from which
606 spherical particles with diameters from 86 – 104 \AA were proposed [see equation (4)]. These values were

607 heavily dependent on the choice of solvent and concentration. Dilution in benzene had little effect,
608 while dilution with decalin led to an increase in particle size, suggesting that the latter is a poor solvent
609 for asphaltenes.

610 Herzog et al.⁸⁵ used SAXS to investigate asphaltenes obtained from 3 geological sources dispersed
611 in benzene or maltenes. The authors used the power law at low scattering angles to characterize particle
612 morphology. The difference between experimental data and the theoretical model was accounted for by
613 porosity within asphaltene particles (ca. 80%). Although quantitative particle size analysis was not
614 presented, this approach indicated the presence of relatively large, porous disks, calculated to have mean
615 radii exceeding 800 Å.

616 Ravey et al. were the first to perform SANS on asphaltenes isolated from 5 different sources of
617 crude oil.⁶⁹ Analyses were conducted in d_8 -THF, d_6 -benzene or d_5 -pyridine after fractionation using
618 preparative gel permeation chromatography (GPC). Spheroid and disk-like scattering models were
619 applied to calculate R_g and M_w values. R_g values varied between 30 Å or 70 Å depending on specific
620 asphaltene fraction, and satisfactory fits were achieved using either a spheroid model (with diameters
621 ranging from 80 to 190 Å) or a disk model (with diameters ranging from 130 to 850 Å). Meanwhile,
622 the mean spheroid or disk thickness was calculated to lie in the range of 4.5 to 9.0 Å, which is lower
623 than most L_c values determined by XRD studies of nanoaggregate dimensions (Table 1). These
624 structural parameters depended strongly on the choice of solvent but were independent of the geological
625 source of asphaltene and its concentration in solution. For example, particle diameters determined in
626 d_6 -benzene (a non-polar solvent) were more than an order of magnitude larger than those calculated
627 when using more polar solvents such as d_8 -THF or d_5 -pyridine.

628 Sheu et al.⁷² reported that SANS data recorded for asphaltene dispersions in d_8 -toluene/ d_5 -pyridine
629 could be fit to a spherical particle model with a Schultz distribution function. Surprisingly, spherical
630 particle radii derived from these analyses (30.8 – 32.4 Å) were found to be independent of solvent
631 composition or asphaltene concentration. This lack of particle growth with concentration was attributed
632 to the packing constraints in asphaltenes preventing further aggregation. Sheu followed up with a study
633 of temperature-dependent aggregation behavior in toluene, adopting both monodisperse cylinders and

634 Schultz distribution of spherical particles models.⁷⁰ Better fits were achieved for the latter model, and
635 particle radii were found to be relatively constant with both temperature and concentration. The Schultz
636 model also allowed polydispersity to be estimated, and this value was found to decrease significantly
637 with both increasing temperature and concentration, suggesting that some larger aggregates dissociated
638 whilst smaller particles remain unchanged. The authors concluded that the significant polydispersity in
639 asphaltenes precludes the use of Guinier-type analysis that is commonly used for asphaltene particles.
640 The Schultz distribution model was also applied to SAXS data recorded for four different asphaltenes
641 dispersed within the non-asphaltic portion of respective crude oils.⁷⁴ Mean particle radii ranged from
642 30 to 60 Å (polydispersity = 12 – 20%) with no apparent correlation with the heteroatom or aromatic
643 content of such samples. However, dilution with crude oil-derived solvent generally produced finer
644 particles.⁷²

645 Thiyagarajan et al. reported similar results when conducting variable temperature SANS studies on
646 asphaltenes dispersed in deuterated 1-methylnaphthalene.⁹⁹ Guinier analysis indicated that R_g was
647 reduced significantly from ca. 47 Å to 12 Å on heating from 25 °C to 400 °C. Power law analysis at
648 low q indicated the presence of rod-like particles at room temperature, with modelling suggesting mean
649 rod lengths of 500 Å. Shorter rods were formed at higher temperature, at which ellipsoidal models were
650 required to fit the data. Only spherical particle models provided satisfactory fits to SANS patterns
651 recorded at 400 °C. Overall, this study indicates that asphaltene particles seem to undergo a gradual
652 morphological transition from cylinders to spheres on heating.

653 *Hierarchical structure*

654 The size distributions at different lengthscales in asphaltenes were addressed by Liu et al. through
655 SANS analysis.⁸¹ Models were applied to derive fractal dimensions and the mean number of primary
656 particles per cluster as a function of asphaltene concentration in toluene. At most concentrations, d_f was
657 determined to be 3.0 but a minimum value of 1.8 was calculated at intermediate concentration.
658 Interestingly, the mean number of particles per cluster increased from 20 up to a maximum value of 60
659 over the same concentration range. The authors concluded that fractal clusters were only present at

660 asphaltene concentrations above 40% w/w. Preparation of highly concentrated dispersions ($\geq 80\%$ w/w)
661 led to phase inversion, producing toluene droplets dispersed within an asphaltene matrix.*

662 Fenistein et al. also used SANS to study the hierarchical structure of asphaltene aggregates.¹⁰⁰
663 Asphaltenes extracted from either Safaniya vacuum residue or an asphaltene-rich crude oil (with the
664 latter comprising a higher aromatic fraction) were dispersed in various deuterated heptol mixtures. The
665 Zimm approximation was used to provide R_g values, which increased at higher d₁₆-heptane fraction
666 for both types of asphaltenes (from either 60 to 200 Å from Safaniya vacuum residue or from 70 to 144
667 Å for the asphaltene-rich crude oil). However, the superposition of all SANS patterns at higher q
668 suggested that essentially the same primary aggregates (for which $R_g < 50$ Å) were present in all cases.
669 Fractal dimensions were calculated from both a master plot of R_g vs. M_w , and by power law analysis in
670 the Porod region, with both approaches producing d_f values of around 2.0 to 2.2. These values indicated
671 open fractal structures with solvent-rich internal structures, which was consistent with the effective
672 molecular volumes determined by viscometry. However, it was recognized that fractal aggregation
673 processes were likely to continue well beyond the “few hour” timescale of the SANS experiments. The
674 authors later used SAXS and SANS in conjunction with DLS to study the evolution of asphaltene
675 morphology in heptol mixtures *in situ*.⁸⁸ Distinct regimes were observed depending on heptane ratio,
676 with solvated fractals observed at low heptane fraction, and large compact structures apparent with
677 increasing heptane. USAXS analysis showed that the larger fractal structures observed for asphaltenes
678 powders also existed when dispersed within the “natural” maltene solvent.

679 Roux et al. used SANS analysis to investigate concentration-dependent asphaltene aggregation in
680 d₈-toluene using Guinier and Zimm approximations.⁷⁸ Values from Zimm were consistently higher from
681 Guinier, which was attributed to fitting the upturn in scattering observed at low q . Both methods showed
682 that, contrary to earlier studies,^{70, 72} increasing the asphaltene concentration led to lower apparent M_w
683 and R_g values. Furthermore, increasing the temperature from 8 °C to 73 °C reduced the degree of
684 aggregation and resulted in a systematic reduction in R_g from 80 to 50 Å. A plot of R_g vs. concentration
685 showed that dilute, semi-dilute and concentrated regimes existed, and that an overlap concentration
686 could be observed. Above this overlap concentration, model fitting effectively measured concentration

687 fluctuations rather than R_g of individual particles.* A plot of M_w vs. R_g from data collected over all
688 concentrations and temperatures had a gradient of 1.9, which indicated the presence of solvent-swollen
689 fractal aggregates.

690 Tanaka et al. used SANS to study three asphaltenes in three solvents (deuterated decalin, 1-
691 methylnaphthalene and quinolone) at 25 °C, 150 °C, 300 °C and 350 °C to produce an extensive set of
692 structural data.¹⁰¹ Each pattern was fitted using the Guinier approach modified for an ellipsoid of
693 rotation or solid sphere. R_g was calculated to be highest in decalin and lowest in 1-methylnaphthylene,
694 with quinolone exhibiting intermediate sizes for all asphaltenes. Lower R_g values were also observed at
695 higher temperatures. At 25 °C, a high aspect ratio prolate ellipsoid model provided the best data fit.
696 However, at elevated temperatures more satisfactory data fits were obtained using a solid sphere model.
697 Surface fractal dimensions were calculated by subtracting the power law obtained at low q from 6 ($d_s =$
698 $2d_f - P$, where $d_f = 3$), giving d_s values ranging from 2.72 at 25 °C to 2.42 at 350 °C. This was interpreted
699 as evidence for smoother particle surfaces at higher temperatures, although fractal networks were only
700 observed for one asphaltene. This particular sample also exhibited a high tendency to generate coke,
701 suggesting that the propensity to form higher order fractal structures may be related to asphaltene drop-
702 out in an industrial context.

703 Mason and Lin time-resolved SANS to address another direct industry problem: the formation of
704 precipitates on mixing two oils with significantly different solvation power for asphaltenes (e.g., Syrian
705 crude oil and British paraffinic oils).²¹ After mixing various volume fractions of the two oils, smaller
706 particles were observed over time when employing lower volume fractions of the asphaltene-rich crude
707 oil, suggesting a higher degree of dispersion. Mixtures containing higher fractions of asphaltene-rich
708 crude oil exhibited relatively constant particle size over time. In addition, surface scattering power law
709 exponents increased more slowly over the course of a week for colloidal dispersions prepared using
710 higher asphaltene fractions. Such data could help to understand the aggregation kinetics and make
711 estimations of repulsive potential barriers between asphaltene particles. Cosultchi et al. also studied the
712 aggregation kinetics over longer timescales upon addition of either toluene or THF to isolated powders
713 from two different asphaltene sources.⁹¹ After the longest reported timescale of one month, the R_g was

714 $161 \pm 2 \text{ \AA}$ for both types of asphaltenes in each solvent. However, immediately after solvent addition
715 the R_g ranged from 192 \AA (THF) to 255 \AA (toluene). Particle morphologies were also deduced from
716 Kratky plots and distance distribution functions, where initially spherical particles were produced in
717 THF, and either spheres or fibres were formed in toluene. Fractal dimensions calculated by power law
718 analysis tended to increase over time and were higher for asphaltene dispersions in toluene than THF.

719 Espinat et al. conducted temperature and pressure-dependent SAXS and SANS studies of
720 asphaltene dispersions in toluene/ d_8 -toluene in an attempt to mimic the conditions experienced by crude
721 oils during their refinery and transport.⁹² In accordance with a prior study by Tanaka et al.,¹⁰¹ these
722 workers found that Zimm analysis of the SANS data yielded R_g values that decreased from 65 \AA at 30
723 $^\circ\text{C}$ to 35 \AA at $290 \text{ }^\circ\text{C}$. However, full molecular dissolution was not observed even at the highest
724 temperatures, while increasing the applied pressure up to 240 bar had no discernible effect on the
725 aggregate morphology. SAXS analysis at $10 \text{ }^\circ\text{C}$ indicated the presence of relatively large aggregates
726 with a fractal dimension of approximately 2. The particles formed on cooling were comparable in size
727 to those formed by solvent-induced flocculation in a previous study (i.e. $R_g > 100 \text{ nm}$).¹⁰⁰ It was
728 proposed that lowering the solution temperature reduced the degree of solvation while increasing the
729 strength of asphaltene interactions, thus favoring the formation of larger particles.

730 Gawrys and Kilpatrick evaluated various scattering models for SANS data recorded for three
731 different asphaltenes dispersed in d_8 -toluene, d_8 -toluene/ d_4 -methanol or d_8 -toluene/ d_{16} -heptane.⁷⁷ Such
732 approaches included Guinier approximation, small-particle mass-fractal, monodisperse models
733 (spheres, prolate cylinders, oblate cylinders) and Schultz polydisperse models (spheres and oblate
734 cylinders only). The best model fit was obtained for oblate cylinders with a polydisperse radius.
735 Interestingly, the particle dimensions depended on the asphaltene source, with more sulfur-rich
736 molecules forming cylinders of smaller mean radii and length, suggesting that the presence of such
737 heteroatoms disrupts π - π^* stacking. Meanwhile, increasing the n -heptane fraction within the heptol
738 solvent led to the formation of larger cylinders. In a follow-up study, Gawrys et al. applied several
739 SANS models to study the solvent entrainment within asphaltene particles.⁷⁶ By modelling the scattered
740 intensity, it was found that greater aggregation occurred when increasing the n -heptane content of heptol

741 mixtures. Polydisperse cylinder models once again produced the best fit to the data relative to Guinier,
742 Zimm, small particle mass fractal. Fractal dimensions were calculated using this latter model, which
743 overcame some of the limitations of techniques used in prior studies. In particular, the M_w vs R_g and
744 Porod gradient approaches favored by earlier workers were considered to require too many assumptions.
745 Depending on the asphaltene chemistry and the solvent conditions, the mean fractal dimensionality was
746 determined to lie between 2.2 and 3.0, with changes in surface roughness being considered to play a
747 key role. Model fits for the primary nanoaggregates indicated that asphaltenes with larger core diameters
748 usually formed thicker stacks, and polydispersity was insensitive to the aggregate size. By calculating
749 apparent M_w values, solvent entrainment within aggregates was estimated to lie in the range of 20 –
750 50% (v/v) depending on the aggregate size.

751 Headen et al. utilized USANS (here named very small-angle neutron scattering, V-SANS) in
752 combination with conventional SANS to examine asphaltenes dispersed in either crude oil or d_8 -toluene
753 at length scales of up to 0.45 μm .⁷³ Unfortunately, poor neutron contrast in crude oil led to weak
754 scattering and hence relatively noisy data for asphaltene dispersions. Nevertheless, Beaucage
755 parametrization¹⁰⁶ and Zimm⁷¹ approximation were employed to calculate primary particle R_g between
756 30 to 50 \AA , which are comparable to values reported for different SAS models and in model solvents
757 from other studies (Table 2 and 3). Satisfactory form factor model fits were achieved for rod-like
758 particles with radii of 16 – 22 \AA and mean lengths ranging from 117 to 137 \AA .¹⁰⁷ Higher temperatures
759 led to smaller R_g values and lower fractal dimensions for these primary particles, but analysis of the low
760 q regime indicated that the size of larger aggregates was only weakly temperature-dependent. A
761 reduction in fractal dimension of the primary aggregates from 3 to 1.8 signified the formation of less
762 dense structures at higher temperatures. However, weaker scattering was observed in the low q regime
763 at higher temperature, indicating fewer large insoluble components were present. Based on these
764 observations, the authors proposed that there were distinct populations of smaller and larger fractal
765 structures, with only 2% of asphaltene molecules existing within larger aggregates at 20 °C.

766 Turikov et al. reported similar R_g values for asphaltene particles dispersed in a range of crude oils
767 and in toluene. However, the relative fractions of large and small particles differed significantly after

768 accounting for the size polydispersity.⁹³ In particular, a major asphaltene particle population ($R_g \sim 80$
769 Å) that was present in all crude oil samples was absent for asphaltene dispersions prepared using
770 toluene. It was concluded that caution should be exercised when characterizing asphaltene particles in
771 model solvents such as toluene because such particle size distributions may differ significantly from
772 those found in crude oil.

773 Hoepfner and co-workers published two reports shedding further light on the soluble and
774 insoluble asphaltene populations.^{52, 103} In the first study, SANS was used to study drop-out upon addition
775 of d_{16} -heptane to asphaltene particles dispersed in either d_8 -toluene or crude oils.¹⁰³ By measuring the
776 scattered intensity at high q , SANS was used to estimate the reduction in the ‘soluble asphaltene’
777 fraction that occurs on addition of n -heptane. The fractal dimensionality calculated from power law in
778 the Porod region was ca. 1.23 – 1.98 for the ‘soluble’ primary asphaltenes, and 2.12 – 2.50 for larger
779 asphaltene aggregates/precipitates, although there was no systematic correlation of these values with
780 the volume fraction of n -heptane. R_g and M_w values calculated for primary nanoaggregates were most
781 strongly affected for one crude oil, increasing from 15 Å to 43 Å on addition of 30% w/w n -heptane.
782 The authors proposed that the asphaltene fraction with lowest solubility in n -heptane were the strongest
783 neutron scatterers within a given crude oil dispersion. In a follow-up paper, the same team utilized both
784 SANS and SAXS, in combination with XRD, to study asphaltenes at various concentrations in three
785 good solvents (THF, toluene or 1-methylnaphthalene).⁵² THF was found to solubilize the highest
786 fraction of asphaltenes but insoluble clusters were observed even at the lowest asphaltene
787 concentrations in all three solvents. Using the Zimm approximation, larger R_g values were calculated at
788 higher asphaltene concentrations in each solvent, concomitant with the presence of a higher fraction of
789 insoluble clusters. Moreover, all such data fell on the same R_g vs. M_w master plot, from which a mean
790 fractal dimension of 1.7 was calculated. The authors discussed various ways in which residual water
791 could affect the degree of aggregation and scattering analysis, and the need to use dry solvents in such
792 experiments was emphasized.

793 Morimoto et al. used SAXS to characterize the morphology of asphaltene in toluene,
794 toluene/pentane (with 10% pentane v/v) and bromobenzene. Bromobenzene is considered to be the best

795 for asphaltene on the basis of Hansen solubility parameter relative to asphaltene ($\Delta\delta$).⁹⁵ R_g values
796 calculated using the Zimm approximation were smaller in toluene than for toluene/pentane mixture, and
797 increased with asphaltene concentration, which is consistent with Hoepfner's study.⁵² However, in
798 bromobenzene it was only possible to estimate R_g for the primary nanoaggregates at the highest
799 concentration owing to absence of any scattering features at lower concentrations. Exceptionally, large
800 fractal structures with sharp interfaces existed at all asphaltene concentrations in bromobenzene, as
801 indicated by a gradient of -4 in the low q region. The authors proposed that the degree of asphaltene
802 aggregation in this solvent differed significantly from the Yen-Mullins model.¹² More specifically, the
803 molecular components that are normally located at the surface of asphaltene particles are molecularly
804 dispersed in bromobenzene, whereas the core-forming molecules remain dispersed as rigid aggregates.
805 A useful positive correlation between $\Delta\delta$ and either R_g or M_w was observed, from which particle size
806 could be estimated for a given asphaltene at a particular concentration in a given solvent.

807 Hoepfner and co-workers later utilized simultaneous SAXS and USAXS to follow morphological
808 changes in soluble and insoluble asphaltene aggregates during the *n*-heptane-induced precipitation from
809 toluene.⁶⁶ In toluene, soluble aggregates with an R_g of 10 Å were detected that remained relatively
810 unchanged over experimental time scales. Initially, the R_g of these soluble aggregates increased with
811 the volume of added *n*-heptane, but then a reduction in R_g was observed above 43% *n*-heptane as a
812 larger fraction of asphaltenes became insoluble and hence were no longer detected within the same q
813 range. The fractal dimensions of the soluble aggregates were determined to be 1.6 by two different
814 analytical methods. *In situ* SAXS/USAXS analysis after addition of 46% *n*-heptane indicated that
815 significant morphological changes were only observed for the insoluble clusters (i.e. within the low q
816 USAXS region). R_g and M_w values for these insoluble clusters increased more rapidly over time, which
817 was suggested to be the result of a nascent precipitate phase seeding further precipitation. During this
818 experiment, the fractal dimension of the insoluble clusters (measured by power law analysis) increased
819 from 3.6 to 4.0, suggesting that the initially rough surface fractals became smoother and formed sharp
820 interfaces with the surrounding medium.

821 *Fractionation*

822 Various studies have investigated how the morphology of asphaltene is affected by its
823 fractionation. Fenistein and Barré separated various asphaltene dispersions by ultracentrifugation in
824 toluene and studied the asphaltene morphology of resulting fractions using SAXS.⁸⁹ Ultracentrifugation
825 into various mass fractions produced particles with R_g values ranging from 33 to 252 Å, thus
826 demonstrating the highly polydisperse nature of asphaltene aggregates. Both R_g vs. M_w plots and power-
827 law analysis at intermediate q were used to estimate fractal dimensions in the region of 2. The
828 mechanism and kinetics of asphaltene aggregation were also discussed, and it was postulated that a
829 balance existed between short-range attractive interactions between the insoluble fused aromatic cores
830 and longer range steric repulsion between solvated aliphatic chains.

831 Barré et al. proceeded to use fractionation by ultracentrifugation as a means to study the relationship
832 between the length scales measured by SAXS and the solution viscosity of asphaltenes.⁶⁷ The R_g of
833 primary asphaltene aggregates was calculated by Zimm fitting and found to be independent of
834 concentration in toluene. The gradient of 2.1 determined at high q was attributed to either fractal
835 structures or disk-shaped particles, with differences in scattering at low q being taken to indicate
836 concentration-dependent changes in the larger scale aggregate morphology. The scaling of viscosity
837 with concentration was not consistent with the presence of disk-shaped particles but could be
838 rationalized by assuming that asphaltene formed hard sphere aggregates swollen with interstitial
839 solvent. The same authors subsequently adopted a combination of SAXS and SANS to demonstrate that
840 solvent trapped within asphaltene fractal aggregates could account for the concentration dependence of
841 the solution viscosity.⁶⁵ SANS and neutron reflectivity experiments were also performed on asphaltenes
842 adsorbed onto solid surfaces and at oil-water interfaces. In such cases R_g values were found to be
843 comparable to those determined in solution, suggesting that asphaltene aggregates formed monolayers
844 by adsorption at interfaces.

845 Such a combination of SAXS and SANS was later used by Eyssautier et al. to analyze a range of
846 asphaltenes in dilute toluene/ d_8 -toluene solutions.⁶⁴ The data obtained from these two techniques
847 compared well at low q (i.e. for longer length scales) but oscillations within the SANS data at high q

848 indicated fine structural details that were not detectable by SAXS (see Figure 4). Contrast variation
849 techniques were employed for SANS analysis. This involved systematic variation of the H/D isotopic
850 ratio to rigorously assess the quality of the data fits obtained when using sphere and cylinder models,
851 which are indistinguishable according to the SAXS data. The cylindrical (or disk) model provided the
852 best fit to the SANS patterns over a range of H/D ratios, with the corresponding calculated dimensions
853 suggesting an aromatic core radius of 18.2 Å, an aliphatic shell thickness of 14.4 Å, and a disk height
854 of 6.7 Å. In general, these structural parameters are larger than those expected based on the modified
855 Yen model.¹⁴ SLD calculations modelled from SANS data confirmed that the aliphatic shell density
856 was far greater than that expected for an *n*-alkane, suggesting the formation of a dense shell as a result
857 of the close-packed stacks of aromatic cores. This team also characterized the temperature and
858 concentration-dependent asphaltene morphology when such particles were dispersed in the maltenes
859 from which they were isolated.⁹⁴ Again, lower R_g and M_w values were obtained at higher temperatures.
860 This behavior was interpreted as evidence for the desorption of resins from the surface of asphaltene
861 particles and/or cluster dissociation, which is consistent with the observed viscometric properties.

862 Eyssautier et al. separated asphaltenes into ‘filtrates’ and ‘retentates’ using porous membranes with
863 a range of pore sizes.⁶³ Asphaltene dispersions in crude oil-based solvents (i.e. maltenes) were subjected
864 to SAXS and USAXS analyses. As expected, lower R_g and M_w values were obtained when using
865 membranes with smaller pores and also at higher temperatures. Moreover, it was clear that asphaltene
866 aggregates were present up to 300 °C. Such observations suggest that irreducible primary asphaltene
867 nanoaggregates are present under all conditions, including those corresponding to refinery processing.
868 Fractal dimensions (calculated from M_w vs R_g plots) showed two regimes at differing length scales,
869 suggesting fractal structures at both the nanoaggregate and cluster length scales. USAXS analysis
870 enabled larger particles to be observed at low q and confirmed that membrane retentates contained large
871 mineral particles that were absent in the filtrates. Furthermore, the fractal dimension data suggested
872 similar structural dimensions for asphaltenes dispersed in maltenes as toluene (observed in a prior study
873 from the same group).⁶⁴ This is an important result, because it suggests that such ‘model’ oils are indeed
874 useful mimics for understanding the behavior of asphaltenes within crude oil.

875 Ballard et al. separated asphaltenes according to their differing surface activities by isolating the
876 fraction that adsorbed at the interface of a toluene/water mixture.¹⁰⁴ This so-called ‘interfacially-active
877 asphaltene’ (IAA) was compared to the original whole asphaltenes (WA) and the (interfacially-inactive)
878 remaining asphaltene (RA) fractions by SANS analysis. A shape-independent broad peak model was
879 applied to SANS data to obtain a characteristic length, which was assumed to correspond to
880 nanoaggregate radius. This parameter was approximately twice as large for IAA (60 Å) as for RA (29
881 Å). Meanwhile, the power law component corresponding to the fractal dimension was smaller for IAA
882 than for RA, suggesting a less compact structure for the former species. Variations in chemical
883 composition (particularly sulfur, oxygen and nitrogen contents) between IAA and RA were suggested
884 to be responsible for these morphological differences. Moreover, the authors postulated that the
885 presence of S=O and C-O/C=O groups should strongly influence the aggregation mechanism and the
886 resulting nanoaggregate morphology.

887 *Additives*

888 Systems in which additional molecules are mixed with asphaltene to influence their aggregation
889 and morphology have been studied using scattering techniques on numerous occasions. For example,
890 Chang and Fogler used SAXS to study the morphology of asphaltenes prepared in the presence of
891 amphiphiles that stabilize against asphaltene precipitation: p-nonylphenol (NP) and p-
892 dodecylbenzenesulfonic acid (DBSA).⁸⁶ Interaction between such putative stabilizers and the
893 asphaltene aggregates was proven by showing that the X-ray scattered intensity for a solution containing
894 both asphaltene and stabilizer was higher than the sum of the scattering from solutions comprising the
895 individual components. Samples were prepared in toluene, *n*-dodecane or *n*-heptane, and based on the
896 similarity between the corresponding SAXS curves it was concluded that the two stabilizers were
897 equally effective at preventing aggregation in all solvents. R_g values were estimated using the Guinier
898 approximation: aggregate sizes increased from 37 Å in the absence of any stabilizer up to 42 Å for NP
899 and 75 Å for DBSA, respectively. Analysis of pair distance distribution functions, $P(r)$, which gives a
900 probability of finding two scattering entities at a distance r , indicated that r values began to increase

901 above a critical DBSA concentration, suggesting that aggregation was actually promoted at high
902 stabilizer loadings.

903 Spiecker et al. studied the effect of adding resin fractions derived from crude oil on asphaltene
904 aggregation in various heptol mixtures.¹⁷ SANS analysis with Guinier fitting was used to monitor a
905 reduction in aggregate size from 40 – 60 Å to 10 – 20 Å on addition of up to 10% resin to four different
906 asphaltenes. Furthermore, much less intense scattering in the low q region was observed in the presence
907 of resins, which suggests that a smaller fraction of insoluble clusters formed. As in the study by Chang
908 and Fogler, neutron scattering from mixtures exceeded that of the individual components, indicating
909 physical interactions between the resin and asphaltene particles. Resins interacted most strongly with
910 more polar asphaltene fractions and it was proposed that these fractions were most prone to form
911 aggregates in solution and also adsorb at interfaces. A follow-up study examined the influence of such
912 resins on asphaltene precipitation in more detail.¹⁰² The mean correlation length and M_w varied
913 depending on the crude oil source, choice of solvent, and asphaltene fraction (i.e. nanoaggregates vs.
914 clusters). Asphaltenes with reduced aromatic character generally formed smaller aggregates. However,
915 the resin content had a significant influence on the correlation length, which was reduced from 110 Å
916 to 38 Å. Fractal dimensions ranged from 1.7 to 2.1 in the absence of resin, increasing to a limiting value
917 of 3.0 at an asphaltene/resin ratio of 2.0. This suggests that the asphaltene particles became saturated
918 with resin at this ratio. The authors proposed that the resin molecules intercalated between asphaltene
919 molecules, leading to the formation of denser structures with greater fractal character. The smallest
920 observed aggregates (correlation length ≤ 20 Å) were denoted ‘irreducible oligomers’ that could not be
921 further broken up, as observed in many other studies.

922 Larichev et al. studied the development of asphaltene structure that occurred after addition of n -
923 heptane to six crude oils that differed in their resin content.⁹⁶ Data fitting produced both R_g and $R_{g,cross}$
924 (particle cross-section) with the $R_{g,cross}/R_g$ ratio providing information regarding the particle anisotropy
925 or mean aspect ratio. For each oil, R_g increased rapidly within the first hour before reaching a plateau,
926 but the increase in the $R_{g,cross}/R_g$ ratio differed significantly between crude oils. Rapid increases were
927 observed within 1 h for crude oils with the lowest resin content, whereas resin-rich oils exhibited much

928 slower growth over 72 h. The same authors subsequently studied the addition of the ‘nitrogen-base’
929 components of resins on primary nanoaggregates and secondary clusters, both in the solid state and in
930 toluene solution.⁹⁷ In the solid state, the position of a broad scattering maximum was used to estimate a
931 primary cluster size of 36 Å, while Guinier analysis was used to characterize the R_g of the secondary
932 clusters. High resin contents reduced the R_g of the secondary clusters from 150 to 56 Å and led to
933 attenuation of the broad SAXS correlation peak, which was interpreted in terms of more loosely packed
934 primary particles. The resins also reduced the fractal dimensions of the primary nanoaggregates (as
935 determined by power law analysis), suggesting their degradation into disordered diffuse fragments.

936 Sheu et al. studied the effect of adding sodium dodecylsulfate (SDS) on asphaltene particle size
937 using SANS.⁷⁵ The neutron scattered intensity at low q was reduced in the presence of SDS, which is
938 consistent with the formation of fewer insoluble clusters. However, the size of the primary aggregates
939 was largely unchanged, suggesting that these fundamental building blocks remain intact in the presence
940 of such additives.

941 Padula et al. correlated asphaltene morphology with rheological studies performed in the presence
942 of additives such as co-solvents, surfactants and polymers.⁷⁹ Unified models were applied to SAXS data
943 to describe the asphaltene morphology over a range of concentrations in heptol mixtures and maltenes.
944 For two different sources of asphaltene in both toluene and *n*-heptane, there was little effect of
945 concentration on R_g suggesting the primary aggregates remained constant regardless of the solvent
946 composition. Meanwhile, more significant size effects were observed in the presence of additives. In
947 particular, addition of a surfactants such as DBSA or nonylphenol ethoxylate significantly reduced the
948 asphaltene R_g for the aromatic-rich crude oil. This is consistent with prior studies that demonstrated the
949 ability of suitable additives to stabilize asphaltene dispersions and prevent their precipitation.^{34, 86, 108}
950 Although no quantitative data fitting was attempted at low q , the appearance of strong scattering
951 suggested the presence of relatively large objects ($R_g > 90$ nm). Fractal dimensions determined by power
952 law analysis of SAXS patterns varied significantly depending on the origin of the crude oil, with
953 aromatic-rich oils generally exhibiting less fractal character.

954 The Hoepfner group conducted *in situ* experiments to study the effect of inhibitors on asphaltene
955 aggregation using USAXS.⁹⁸ So-called ‘K values’ were derived from the X-ray scattered intensity to
956 describe the proportion of insoluble asphaltenes in the presence of inhibitors relative to that in the
957 absence of any inhibitor, whereby lower ‘K values’ indicate more effective stabilization. *n*-
958 Dodecylphenol (DDPh) prevented any precipitation when present at sufficiently high concentration
959 (5000 ppm), while other additives merely delayed the onset of precipitation. The effect of inhibitor on
960 both soluble (high q region) and insoluble (low q region) fractions was studied. The power law at low
961 q increased over time from 2.9 to 3.2 in the absence of inhibitor, indicating evolution from a dense mass
962 fractal to a rough surface fractal. The presence of inhibitors reduced this increase in d_f to a final fractal
963 dimension of just 2.3 at the highest DDPh loading. It was concluded that inhibitors prevented the
964 formation of rougher particles that had a higher propensity to aggregate. The mean radius of gyration
965 of the nanoaggregates was determined by Guinier analysis. Only the highest concentration of DDPh
966 inhibitor (5000 ppm) led to a significant reduction in R_g (from ~ 100 Å to ~ 75 Å).

967 Knudsen et al. examined interactions between asphaltenes and a commercial Pluronic-type
968 triblock copolymer.¹⁰⁵ Increasing the fraction of deuterated *n*-heptane within heptol solutions led to an
969 increase in R_g and M_w as determined by SANS. Neutron reflectometry studies were then conducted on
970 surfaces on which asphaltene had been deposited. This asphaltene layer was found to be 8 Å thinner in
971 the presence of the Pluronic copolymer. Moreover, this surface was discernibly rougher, which was
972 consistent with the reduced adsorbed amount indicated by quartz crystal microbalance studies.
973 However, this study also suggested that the amphiphilic Pluronic copolymer chains were only weakly
974 incorporated within these layers.

975 **Summary of asphaltene structural information obtained from scattering methods**

976 The various SAXS, SANS, and XRD studies discussed and summarized in Tables 1 – 3 indicate
977 that the structural dimensions of asphaltenes at multiple length scales (depicted in Figure 1) depend on
978 many inter-connected parameters that can be difficult to deconvolute. However, systematic studies have
979 shed some light on various aspects that influence the morphology of these complex materials, including:

980 (i) their chemical structure, (ii) solvent composition, (iii) asphaltene concentration, (iv) solution
981 temperature and (v) the presence of exogenous additives.

982 Given the many structural variables and considerable heterogeneity within an asphaltene dispersion,
983 it is extremely difficult to correlate differences in chemical structure with the aggregate morphology.
984 Nevertheless, the judicious combination of scattering techniques coupled with elemental microanalysis
985 and NMR spectroscopy can provide important insights on both molecular and colloidal length scales.
986 Chemical functionality can vary widely depending on the geological origin of the crude oil from which
987 the asphaltene is derived, as well as the conditions employed for its processing and fractionation.

988 According to XRD analyses reported in the literature, the morphology of asphaltenes depends on
989 their aromatic character,^{44, 45, 47, 54} heteroatom content,^{45-47, 57} and alkyl chain length.^{50, 56} It is generally
990 accepted that their fused aromatic rings lead to intermolecular aggregation via π - π^* interactions.
991 However, other types of non-covalent interactions can also influence the extent of asphaltene
992 aggregation, including hydrogen bonding through heteroatoms and van der Waals forces acting between
993 aliphatic groups. Alternatively, N, O or S atoms can increase the mean stack thickness as a result of
994 stronger intermolecular interactions^{47, 57} or aromatic ring size.⁴⁷ The nature of the aliphatic groups may
995 also influence the degree of stacking: longer chains enable the formation of thicker stacks,⁵⁶ whereas
996 shorter chains promote more efficient molecular packing and hence shorter interlayer distances.⁵⁰
997 Moreover, asphaltenes containing fewer aromatic rings per molecule tend to form relatively disordered
998 amorphous aggregates,⁴⁴ while aromatic rings with fewer substituents can lead to more efficient packing
999 and larger nanoaggregates.⁴⁷ Some studies have begun to examine how differing asphaltene reaction
1000 pathways^{50, 53} can exert a strong influence over asphaltene morphology. For example, heteroatom-rich
1001 asphaltenes appear to follow different oxidation pathways that may lead to more loosely-stacked
1002 aggregates.⁴⁶ Moreover, asphaltene processing protocols that reduce aromatic character produce fewer
1003 molecules per stack and shorter inter-stack distances.^{45, 54}

1004 Fractionation of asphaltenes by preparative gel permeation chromatography,⁶⁹
1005 ultracentrifugation^{67, 89} or membrane filtration⁶³ indicate significant polydispersity within asphaltenes.
1006 However, in most cases such size-based fractions do not differ markedly in terms of their chemical

1007 functionality. Interestingly, the most surface-active asphaltenes tend to contain significantly higher
1008 sulfur and oxygen contents and a higher proportion of aliphatic groups. Larger aggregates with lower
1009 fractal dimensions are formed by such interfacially-active asphaltenes, which has been rationalized in
1010 terms of stronger intermolecular interactions.¹⁰⁴

1011 According to multiple SAS studies, the solvent composition can strongly influence the asphaltene
1012 morphology.^{17, 52, 66, 69, 70, 72, 74-79, 81, 83, 84, 88, 91, 95, 98, 100-105} In general, the Hansen solubility parameter is a
1013 good indicator of asphaltene aggregation behavior. In a good solvent environment (e.g. toluene,
1014 pyridine,^{69, 72} THF,^{52, 69, 91} bromobenzene⁹⁵ or 1-methylnaphthalene^{52, 101}), aggregates tend to be smaller
1015 and also dissociate further on dilution, suggesting relatively weak intermolecular interactions in such
1016 conditions. In the case of ‘heptol’ solvent mixtures, adjusting the *n*-heptane/toluene ratio influences
1017 particle size, with larger amounts of *n*-heptane leading to the formation of larger particles.^{76, 77, 88, 100} On
1018 dilution with *n*-heptane-rich solvent mixtures, larger aggregates are formed as a result of greater
1019 flocculation, the opposite case to a good solvent environment.⁸³ Other non-polar solvents such as
1020 benzene⁸⁵ also promote asphaltene aggregation.

1021 Several studies have examined asphaltenes in their ‘natural’ state within crude oils.^{63, 79, 85, 88, 94}
1022 Again, the difference in Hansen solubility parameter between asphaltene and maltene solvent ($\Delta\delta$) is
1023 the key to understanding their aggregation behavior, as recently discussed by Morimoto et al.⁹⁵ Solvent
1024 quality affects the relative proportions of primary nanoaggregates and fractal clusters,^{52, 66, 103} with the
1025 latter component most likely being responsible for asphaltene ‘drop-out’. Most of these solvent effects
1026 have been elucidated by SAS studies, but XRD analysis of asphaltene dispersions has revealed various
1027 changes within the primary aggregates at the molecular level.⁵²

1028 Various XRD⁴⁸ and SAS^{63, 70, 73, 78, 83, 92, 94, 101} studies have demonstrated that the asphaltene
1029 morphology depends on the solution temperature. For example, larger interlayer distances and fewer
1030 molecules per stack were observed by XRD at higher temperature, leading to smaller primary
1031 aggregates.⁴⁸ This is consistent with the general trend observed in SAS data, which has shown that
1032 smaller particles are formed at higher temperatures.^{63, 72, 73, 78, 92, 94, 101} This temperature-dependent
1033 behavior has been rationalized in terms of stronger attractive forces and weaker solvation at lower

1034 temperatures.⁹² However, increasing to certain temperatures can result in flocculation and precipitation
 1035 of asphaltenes as in thermal de-asphaltene processes.⁵⁴

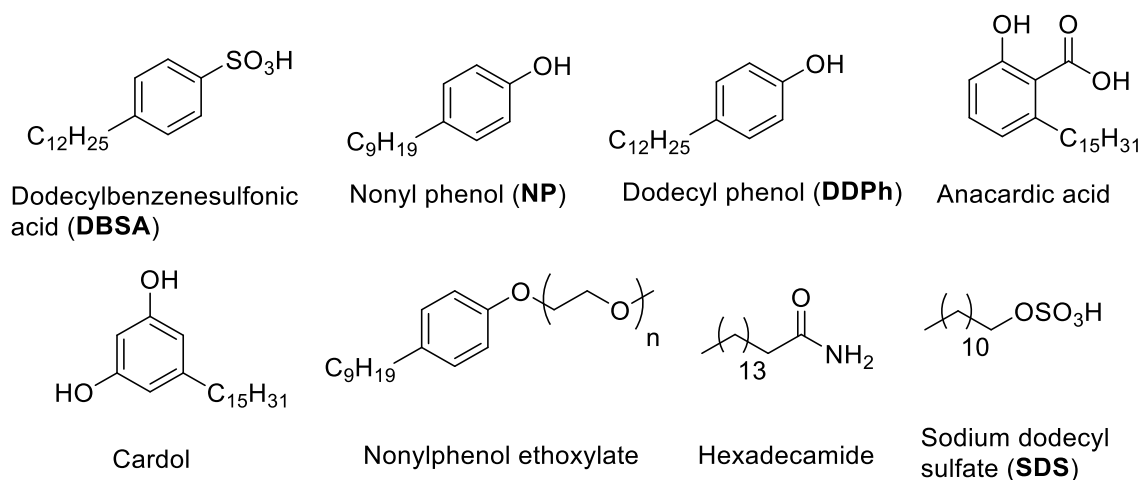


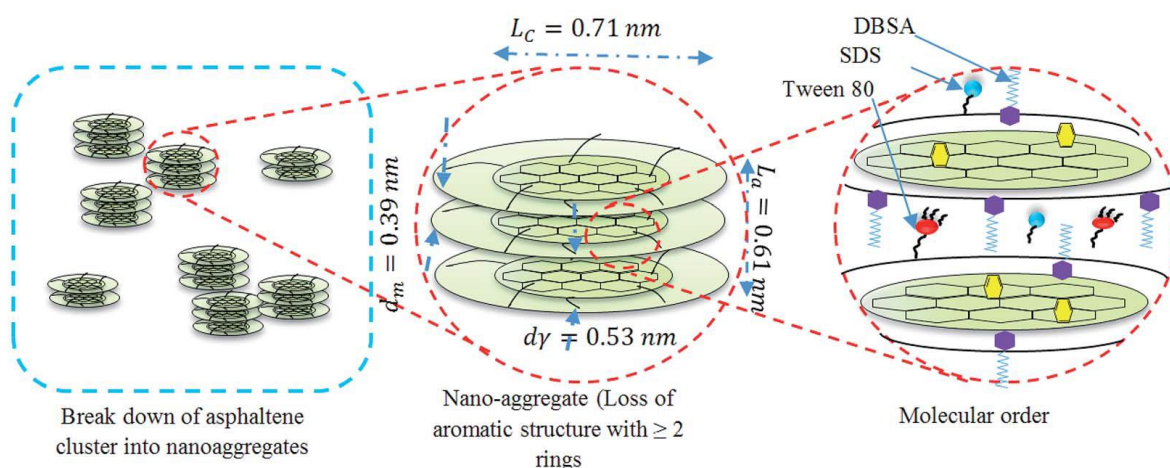
Figure 7: Chemical structures of various additives (otherwise known as dispersants, stabilizers, or inhibitors) that can be used to control asphaltene aggregation according to the literature.

SAS studies also confirm that the asphaltene morphology can be significantly influenced by the presence of additives.^{17, 18, 55, 58, 79, 86, 98, 102} The latter compounds are used to minimize (ideally prevent) asphaltene aggregation and hence alleviate the commercial problems associated with asphaltene drop-out.¹⁰⁹ These additives are typically amphiphilic, comprising non-polar tails and a polar head-group that can interact with specific heteroatoms and functional groups found in asphaltene molecules. Indeed, crude oil contains a fraction known as ‘resins’, which are believed to aid the dispersion of asphaltenes on the colloidal length scale by intercalation within the aromatic stacks of asphaltenes and presentation of their aliphatic tails at the surface of the asphaltene aggregates.¹⁷ Exogenous additives used to control asphaltene aggregation possess some common structural motifs, including benzene rings, polar groups (e.g. alcohols, sulfonates, or ethylene oxide oligomers), and aliphatic chains of various lengths (Figure 7). XRD analyses have shown that such additives increase the mean distance between aromatic rings (d_m), suggesting their intercalation between the stacked polyaromatic rings.^{18, 58} Other studies suggest a reduction in the mean number of molecules per stack and hence the mean stack thickness.^{18, 55} One theoretical study proposed that the interaction of additives with asphaltenes can affect their aromatic

1054 character and therefore their propensity to undergo π - π stacking.⁵⁵ On longer length scales, results of
1055 SAS studies suggest that additives can increase the R_g of asphaltene particles, or even promote their
1056 aggregation at higher concentrations.⁸⁶

1057

1058



1059 **Figure 8:** Schematic cartoons to illustrate the interaction and incorporation of additives between
1060 asphaltene stacks, taken from the literature.¹⁸

1061

1062 Conclusions and Future Outlook

1063 *In situ* SAS analysis is a powerful method to study asphaltene aggregation, which is directly
1064 connected to multiple industrial problems. Nevertheless, the development of more sophisticated
1065 analytical models remains desirable. Since more than one interpretation of any given scattering pattern
1066 may be possible, the combination of SAS with other analytical techniques is crucial to avoid ambiguity
1067 in the structural analysis of asphaltenes. Furthermore, scattering experiments are not always conducted
1068 under relevant 'real-world' conditions, which may limit data interpretation in the context of asphaltene
1069 drop-out. Developing reliable combinations of analytical methodologies that can be consistently applied
1070 to asphaltenes in both the solid state and colloidal dispersions should enable more meaningful
1071 comparison between data reported by different groups, and hence facilitate a deeper understanding of
1072 the relevant structure-property relationships at the molecular length scale. This is also likely to be

1073 important when establishing differences in the behavior of crude oils arising from their differing
1074 geographical sources. In addition, meta-analysis of the structural data already reported in the literature
1075 should provide further insight into the structural correlations between different sources of asphaltene
1076 and their behavior under various conditions. Furthermore, detailed studies of the mechanism(s) of action
1077 of various inhibitors are warranted, not least because such additives are essential to prevent the various
1078 industrial problems associated with asphaltene ‘drop-out’. An enhanced understanding of how to
1079 control asphaltene aggregation is most likely required if their potential application within next-
1080 generation materials is to be realized, such as organic dye sensitized solar cells²⁶, supercapacitors,²⁷
1081 biological imaging,²⁸ and electrocatalysts.²⁹

1082

1083 **References**

- 1084 (1) Palacio Lozano, D. C.; Orrego-Ruiz, J. A.; Barrow, M. P.; Cabanzo Hernandez, R.; Mejía-Ospino,
1085 E. Analysis of the molecular weight distribution of vacuum residues and their molecular distillation
1086 fractions by laser desorption ionization mass spectrometry. *Fuel* **2016**, *171*, 247-252. DOI:
1087 <https://doi.org/10.1016/j.fuel.2015.12.058>. McKenna, A. M.; Blakney, G. T.; Xian, F.; Glaser, P. B.;
1088 Rodgers, R. P.; Marshall, A. G. Heavy Petroleum Composition. 2. Progression of the Boduszynski
1089 Model to the Limit of Distillation by Ultrahigh-Resolution FT-ICR Mass Spectrometry. *Energy & Fuels*
1090 **2010**, *24* (5), 2939-2946. DOI: 10.1021/ef1001502. McKenna, A. M.; Purcell, J. M.; Rodgers, R. P.;
1091 Marshall, A. G. Heavy Petroleum Composition. 1. Exhaustive Compositional Analysis of Athabasca
1092 Bitumen HVGO Distillates by Fourier Transform Ion Cyclotron Resonance Mass Spectrometry: A
1093 Definitive Test of the Boduszynski Model. *Energy & Fuels* **2010**, *24* (5), 2929-2938. DOI:
1094 10.1021/ef100149n. McKenna, A. M.; Donald, L. J.; Fitzsimmons, J. E.; Juyal, P.; Spicer, V.; Standing,
1095 K. G.; Marshall, A. G.; Rodgers, R. P. Heavy Petroleum Composition. 3. Asphaltene Aggregation.
1096 *Energy & Fuels* **2013**, *27* (3), 1246-1256. DOI: 10.1021/ef3018578.
- 1097 (2) McKenna, A. M.; Marshall, A. G.; Rodgers, R. P. Heavy Petroleum Composition. 4. Asphaltene
1098 Compositional Space. *Energy & Fuels* **2013**, *27* (3), 1257-1267. DOI: 10.1021/ef301747d.

- 1099 (3) Speight, J. G.; Wernick, D. L.; Gould, K. A.; Overfield, R. E.; Rao, B. M. L. Molecular Weight and
1100 Association of Asphaltenes: a Critical Review. *Rev. Inst. Fr. Pét.* **1985**, *40* (1), 51-61,
1101 10.2516/ogst:1985004.
- 1102 (4) Fakher, S.; Ahdaya, M.; Elturki, M.; Imqam, A. Critical review of asphaltene properties and factors
1103 impacting its stability in crude oil. *Journal of Petroleum Exploration and Production Technology* **2020**,
1104 *10* (3), 1183-1200. DOI: 10.1007/s13202-019-00811-5.
- 1105 (5) Hosseini-Dastgerdi, Z.; Tabatabaei-Nejad, S. A. R.; Khodapanah, E.; Sahraei, E. A comprehensive
1106 study on mechanism of formation and techniques to diagnose asphaltene structure; molecular and
1107 aggregates: a review. *Asia-Pacific Journal of Chemical Engineering* **2015**, *10* (1), 1-14. DOI:
1108 10.1002/apj.1836 (accessed 2020/04/21).
- 1109 (6) Schuler, B.; Fatayer, S.; Meyer, G.; Rogel, E.; Moir, M.; Zhang, Y.; Harper, M. R.; Pomerantz, A.
1110 E.; Bake, K. D.; Witt, M.; et al. Heavy Oil Based Mixtures of Different Origins and Treatments Studied
1111 by Atomic Force Microscopy. *Energy & Fuels* **2017**, *31* (7), 6856-6861. DOI:
1112 10.1021/acs.energyfuels.7b00805. Schuler, B.; Meyer, G.; Peña, D.; Mullins, O. C.; Gross, L.
1113 Unraveling the Molecular Structures of Asphaltenes by Atomic Force Microscopy. *Journal of the*
1114 *American Chemical Society* **2015**, *137* (31), 9870-9876. DOI: 10.1021/jacs.5b04056.
- 1115 (7) Coelho, R. R.; Hovell, I.; Moreno, E. L.; de Souza, A. L.; Rajagopal, K. Characterization of
1116 Functional Groups of Asphaltenes in Vacuum Residues Using Molecular Modelling and FTIR
1117 Techniques. *Petroleum Science and Technology* **2007**, *25* (1-2), 41-54. DOI:
1118 10.1080/10916460601054198.
- 1119 (8) Sodero, A. C. R.; Santos Silva, H.; Guevara Level, P.; Bouyssiére, B.; Korb, J.-P.; Carrier, H.;
1120 Alfarra, A.; Bégué, D.; Baraille, I. Investigation of the Effect of Sulfur Heteroatom on Asphaltene
1121 Aggregation. *Energy & Fuels* **2016**, *30* (6), 4758-4766. DOI: 10.1021/acs.energyfuels.6b00757.
- 1122 (9) Thomas, M. J.; Jones, H. E.; Palacio Lozano, D. C.; Gavard, R.; Carney, S.; Barrow, M. P.
1123 Comprehensive analysis of multiple asphaltene fractions combining statistical analyses and novel
1124 visualization tools. *Fuel* **2021**, *291*, 120132. DOI: <https://doi.org/10.1016/j.fuel.2021.120132>.
- 1125 (10) Chianelli, R. R.; Siadati, M.; Mehta, A.; Pople, J.; Ortega, L. C.; Chiang, L. Y. Self-Assembly of
1126 Asphaltene Aggregates: Synchrotron, Simulation and Chemical Modeling Techniques Applied to

1127 Problems in the Structure and Reactivity of Asphaltenes. In *Asphaltenes, Heavy Oils, and Petroleomics*,
1128 Mullins, O. C., Sheu, E. Y., Hammami, A., Marshall, A. G. Eds.; Springer New York, 2007; pp 375-
1129 400.

1130 (11) Mullins, O. C. The Asphaltenes. *Annual Review of Analytical Chemistry* **2011**, *4* (1), 393-418.
1131 DOI: 10.1146/annurev-anchem-061010-113849 (accessed 2020/09/01).

1132 (12) Mullins, O. C.; Sabbah, H.; Eyssautier, J.; Pomerantz, A. E.; Barré, L.; Andrews, A. B.; Ruiz-
1133 Morales, Y.; Mostowfi, F.; McFarlane, R.; Goual, L.; et al. Advances in Asphaltene Science and the
1134 Yen–Mullins Model. *Energy & Fuels* **2012**, *26* (7), 3986-4003. DOI: 10.1021/ef300185p.

1135 (13) Dickie, J. P.; Yen, T. F. Macrostructures of the asphaltic fractions by various instrumental methods.
1136 *Analytical Chemistry* **1967**, *39* (14), 1847-1852. DOI: 10.1021/ac50157a057.

1137 (14) Mullins, O. C. The Modified Yen Model. *Energy & Fuels* **2010**, *24* (4), 2179-2207. DOI:
1138 10.1021/ef900975e.

1139 (15) Sirota, E. B.; Lin, M. Y. Physical Behavior of Asphaltenes. *Energy & Fuels* **2007**, *21* (5), 2809-
1140 2815. DOI: 10.1021/ef060634c.

1141 (16) Sirota, E. B. Physical Structure of Asphaltenes. *Energy & Fuels* **2005**, *19* (4), 1290-1296. DOI:
1142 10.1021/ef049795b.

1143 (17) Spiecker, P. M.; Gawrys, K. L.; Trail, C. B.; Kilpatrick, P. K. Effects of petroleum resins on
1144 asphaltene aggregation and water-in-oil emulsion formation. *Colloids and Surfaces A: Physicochemical
1145 and Engineering Aspects* **2003**, *220* (1), 9-27. DOI: [https://doi.org/10.1016/S0927-7757\(03\)00079-7](https://doi.org/10.1016/S0927-7757(03)00079-7).

1146 (18) Alhreez, M.; Wen, D. Molecular structure characterization of asphaltene in the presence of
1147 inhibitors with nanoemulsions. *RSC Advances* **2019**, *9* (34), 19560-19570, 10.1039/C9RA02664A.
1148 DOI: 10.1039/C9RA02664A.

1149 (19) Eskin, D.; Mohammadzadeh, O.; Akbarzadeh, K.; Taylor, S. D.; Ratulowski, J. Reservoir
1150 impairment by asphaltenes: A critical review. *The Canadian Journal of Chemical Engineering* **2016**,
1151 *94* (6), 1202-1217. DOI: 10.1002/cjce.22476 (accessed 2020/09/01).

1152 (20) Alomair, O. A.; Almusallam, A. S. Heavy Crude Oil Viscosity Reduction and the Impact of
1153 Asphaltene Precipitation. *Energy & Fuels* **2013**, *27* (12), 7267-7276. DOI: 10.1021/ef4015636.

1154 Gharfeh, S.; Yen, A.; Asomaning, S.; Blumer, D. Asphaltene Flocculation Onset Determinations for

1155 Heavy Crude Oil and Its Implications. *Petroleum Science and Technology* **2004**, 22 (7-8), 1055-1072.
1156 DOI: 10.1081/LFT-120038711.

1157 (21) Mason, T. G.; Lin, M. Y. Time-resolved small angle neutron scattering measurements of asphaltene
1158 nanoparticle aggregation kinetics in incompatible crude oil mixtures. *The Journal of Chemical Physics*
1159 **2003**, 119 (1), 565-571. DOI: 10.1063/1.1572457 (accessed 2020/10/16).

1160 (22) Subramanian, S.; Simon, S.; Sjöblom, J. Asphaltene Precipitation Models: A Review. *Journal of*
1161 *Dispersion Science and Technology* **2016**, 37 (7), 1027-1049. DOI: 10.1080/01932691.2015.1065418.

1162 (23) Hirschberg, A.; deJong, L. N. J.; Schipper, B. A.; Meijer, J. G. Influence of Temperature and
1163 Pressure on Asphaltene Flocculation. *Society of Petroleum Engineers Journal* **1984**, 24 (03), 283-293.
1164 DOI: 10.2118/11202-PA.

1165 (24) Siddiqui, M. A.; Tariq, S. M.; Haneef, J.; Ali, S. I.; Manzoor, A. A. Asphaltene Stability Analysis
1166 for Crude Oils and Their Relationship With Asphaltene Precipitation Models for a Gas Condensate
1167 Field. In SPE Middle East Oil and Gas Show and Conference, Manama, Bahrain; 2019.

1168 (25) Lin, M. S.; Lunsford, K. M.; Glover, C. J.; Davison, R. R.; Bullin, J. A. The Effects of Asphaltenes
1169 on the Chemical and Physical Characteristics of Asphalt. In *Asphaltenes: Fundamentals and*
1170 *Applications*, Sheu, E. Y., Mullins, O. C. Eds.; Springer US, 1995; pp 155-176.

1171 (26) Abujnah, R. Asphaltene as Light Harvesting Material in Dye-Sensitized Solar Cell: Resurrection
1172 of Ancient Leaves. *Journal of Environmental & Analytical Toxicology* **2016**, 6, 345. DOI:
1173 10.4172/2161-0525.1000345.

1174 (27) Qin, F.; Tian, X.; Guo, Z.; Shen, W. Asphaltene-Based Porous Carbon Nanosheet as Electrode for
1175 Supercapacitor. *ACS Sustainable Chemistry & Engineering* **2018**, 6 (11), 15708-15719. DOI:
1176 10.1021/acssuschemeng.8b04227. Enayat, S.; Tran, M. K.; Salpekar, D.; Kabbani, M. A.; Babu, G.;
1177 Ajayan, P. M.; Vargas, F. M. From crude oil production nuisance to promising energy storage material:
1178 Development of high-performance asphaltene-derived supercapacitors. *Fuel* **2020**, 263, 116641. DOI:
1179 <https://doi.org/10.1016/j.fuel.2019.116641>. Qu, W.-H.; Guo, Y.-B.; Shen, W.-Z.; Li, W.-C. Using
1180 Asphaltene Supermolecules Derived from Coal for the Preparation of Efficient Carbon Electrodes for
1181 Supercapacitors. *The Journal of Physical Chemistry C* **2016**, 120 (28), 15105-15113. DOI:
1182 10.1021/acs.jpcc.6b05136. Pan, L.; Wang, Y.; Hu, H.; Li, X.; Liu, J.; Guan, L.; Tian, W.; Wang, X.;

1183 Li, Y.; Wu, M. 3D self-assembly synthesis of hierarchical porous carbon from petroleum asphalt for
1184 supercapacitors. *Carbon* **2018**, *134*, 345-353. DOI: <https://doi.org/10.1016/j.carbon.2018.04.008>. Pan,
1185 L.; Li, X.; Wang, Y.; Liu, J.; Tian, W.; Ning, H.; Wu, M. 3D interconnected honeycomb-like and high
1186 rate performance porous carbons from petroleum asphalt for supercapacitors. *Applied Surface Science*
1187 **2018**, *444*, 739-746. DOI: <https://doi.org/10.1016/j.apsusc.2018.03.122>.

1188 (28) Zhao, P.; Yang, M.; Fan, W.; Wang, X.; Tang, F.; Yang, C.; Dou, X.; Li, S.; Wang, Y.; Cao, Y.
1189 Facile One-Pot Conversion of Petroleum Asphaltene to High Quality Green Fluorescent Graphene
1190 Quantum Dots and Their Application in Cell Imaging. *Particle & Particle Systems Characterization*
1191 **2016**, *33* (9), 635-644. DOI: 10.1002/ppsc.201600070 (accessed 2020/09/17).

1192 (29) Swaminathan, J.; Enayat, S.; Meiyazhagan, A.; Robles Hernandez, F. C.; Zhang, X.; Vajtai, R.;
1193 Vargas, F. M.; Ajayan, P. M. Asphaltene-Derived Metal-Free Carbons for Electrocatalytic Hydrogen
1194 Evolution. *ACS Applied Materials & Interfaces* **2019**, *11* (31), 27697-27705. DOI:
1195 10.1021/acsami.9b05309.

1196 (30) Evdokimov, I. N.; Losev, A. P. Electrical Conductivity and Dielectric Properties of Solid
1197 Asphaltenes. *Energy & Fuels* **2010**, *24* (7), 3959-3969. DOI: 10.1021/ef1001887.

1198 (31) Kamkar, M.; Natale, G. A review on novel applications of asphaltenes: A valuable waste. *Fuel*
1199 **2021**, 285, 119272. DOI: <https://doi.org/10.1016/j.fuel.2020.119272>.

1200 (32) Song, J.; Rezaee, S.; Guo, W.; Hernandez, B.; Puerto, M.; Vargas, F. M.; Hirasaki, G. J.; Biswal,
1201 S. L. Evaluating physicochemical properties of crude oil as indicators of low-salinity-induced
1202 wettability alteration in carbonate minerals. *Scientific Reports* **2020**, *10* (1), 3762. DOI:
1203 10.1038/s41598-020-60106-2.

1204 (33) Janssen, A.; Zaluzec, N. J.; Kulzick, M. A.; Crosher, T.; Burke, M. G. In situ Analytical TEM of
1205 Asphaltene Formation and Aggregation from Crude Oil. *Microscopy and Microanalysis* **2016**, *22* (S3),
1206 796-797. DOI: 10.1017/S1431927616004839 From Cambridge University Press Cambridge Core.

1207 Janssen, A.; Zaluzec, N.; Kulzick, M.; McMahon, G.; Burke, M. G. In Situ TEM Characterization of
1208 Asphaltene Formation in Crude Oil. *European Microscopy Congress 2016: Proceedings* **2016**, 259-
1209 260, <https://doi.org/10.1002/9783527808465.EMC2016.5922>. DOI:
1210 <https://doi.org/10.1002/9783527808465.EMC2016.5922> (accessed 2020/11/25).

1211 (34) Chang, C.-L.; Fogler, H. S. Stabilization of Asphaltenes in Aliphatic Solvents Using Alkylbenzene-
1212 Derived Amphiphiles. 1. Effect of the Chemical Structure of Amphiphiles on Asphaltene Stabilization.
1213 *Langmuir* **1994**, *10* (6), 1749-1757. DOI: 10.1021/la00018a022.

1214 (35) Soleymanzadeh, A.; Yousefi, M.; Kord, S.; Mohammadzadeh, O. A review on methods of
1215 determining onset of asphaltene precipitation. *Journal of Petroleum Exploration and Production*
1216 *Technology* **2019**, *9* (2), 1375-1396. DOI: 10.1007/s13202-018-0533-5.

1217 (36) Burya, Y. G.; Yudin, I. K.; Dechabo, V. A.; Kosov, V. I.; Anisimov, M. A. Light-scattering study
1218 of petroleum asphaltene aggregation. *Applied Optics* **2001**, *40* (24), 4028-4035. DOI:
1219 10.1364/AO.40.004028.

1220 (37) Dutta Majumdar, R.; Montana, T.; Mullins, O. C.; Gerken, M.; Hazendonk, P. Insights into
1221 asphaltene aggregate structure using ultrafast MAS solid-state ¹H NMR spectroscopy. *Fuel* **2017**, *193*,
1222 359-368. DOI: <https://doi.org/10.1016/j.fuel.2016.12.082>.

1223 (38) Sheu, E. Y. Petroleum Asphaltene Properties, Characterization, and Issues. *Energy & Fuels* **2002**,
1224 *16* (1), 74-82. DOI: 10.1021/ef010160b. Adams, J. J. Asphaltene Adsorption, a Literature Review.
1225 *Energy & Fuels* **2014**, *28* (5), 2831-2856. DOI: 10.1021/ef500282p. He, L.; Lin, F.; Li, X.; Sui, H.; Xu,
1226 Z. Interfacial sciences in unconventional petroleum production: from fundamentals to applications.
1227 *Chemical Society Reviews* **2015**, *44* (15), 5446-5494, 10.1039/C5CS00102A. DOI:
1228 10.1039/C5CS00102A. Zuo, P.; Qu, S.; Shen, W. Asphaltenes: Separations, structural analysis and
1229 applications. *Journal of Energy Chemistry* **2019**, *34*, 186-207. DOI:
1230 <https://doi.org/10.1016/j.jechem.2018.10.004>. Rashid, Z.; Wilfred, C. D.; Gnanasundaram, N.;
1231 Arunagiri, A.; Murugesan, T. A comprehensive review on the recent advances on the petroleum
1232 asphaltene aggregation. *Journal of Petroleum Science and Engineering* **2019**, *176*, 249-268. DOI:
1233 <https://doi.org/10.1016/j.petrol.2019.01.004>. Recent Developments on the Elucidation of Colloidal
1234 Aspects of Asphaltenes and Their Relevance to Oilfield Problems. *Journal of the Brazilian Chemical*
1235 *Society* **2020**, *31*, 230 - 243. Martyanov, O. N.; Larichev, Y. V.; Morozov, E. V.; Trukhan, S. N.;
1236 Kazarian, S. G. The stability and evolution of oil systems studied via advanced methods in situ. *Russian*
1237 *Chemical Reviews* **2017**, *86* (11), 999-1023. DOI: 10.1070/rccr4742. Evdokimov, I. N. Colloidal

1238 Asphaltenes—Non-extinct “Dinosaurs” in Native Petroleum. *Energy & Fuels* **2019**, *33* (9), 8440-8447.
1239 DOI: 10.1021/acs.energyfuels.9b01993.

1240 (39) Yen, T. F.; Erdman, J. G.; Pollack, S. S. Investigation of the Structure of Petroleum Asphaltenes
1241 by X-Ray Diffraction. *Analytical Chemistry* **1961**, *33* (11), 1587-1594. DOI: 10.1021/ac60179a039.

1242 (40) Ergun, S.; Tiensuu, V. Interpretation of the intensities of X-rays scattered by coals. *Fuel* **1959**, *38*
1243 (1), 64-78.

1244 (41) Franklin, R. E. The interpretation of diffuse X-ray diagrams of carbon. *Acta Crystallographica*
1245 **1950**, *3* (2), 107-121. DOI: 10.1107/S0365110X50000264 (accessed 2020/10/15).

1246 (42) Warren, B. E. X-Ray Diffraction in Random Layer Lattices. *Physical Review* **1941**, *59* (9), 693-
1247 698. DOI: 10.1103/PhysRev.59.693.

1248 (43) Schwager, I.; Farmanian, P. A.; Kwan, J. T.; Weinberg, V. A.; Yen, T. F. Characterization of the
1249 microstructure and macrostructure of coal-derived asphaltenes by nuclear magnetic resonance
1250 spectrometry and x-ray diffraction. *Analytical Chemistry* **1983**, *55* (1), 42-45. DOI:
1251 10.1021/ac00252a014.

1252 (44) Christopher, J.; Sarpal, A. S.; Kapur, G. S.; Krishna, A.; Tyagi, B. R.; Jain, M. C.; Jain, S. K.;
1253 Bhatnagar, A. K. Chemical structure of bitumen-derived asphaltenes by nuclear magnetic resonance
1254 spectroscopy and X-ray diffractometry. *Fuel* **1996**, *75* (8), 999-1008. DOI:
1255 [https://doi.org/10.1016/0016-2361\(96\)00023-3](https://doi.org/10.1016/0016-2361(96)00023-3).

1256 (45) Shirokoff, J. W.; Siddiqui, M. N.; Ali, M. F. Characterization of the Structure of Saudi Crude
1257 Asphaltenes by X-ray Diffraction. *Energy & Fuels* **1997**, *11* (3), 561-565. DOI: 10.1021/ef960025c.

1258 (46) Siddiqui, M. N.; Ali, M. F.; Shirokoff, J. Use of X-ray diffraction in assessing the aging pattern of
1259 asphalt fractions. *Fuel* **2002**, *81* (1), 51-58. DOI: [https://doi.org/10.1016/S0016-2361\(01\)00116-8](https://doi.org/10.1016/S0016-2361(01)00116-8).

1260 (47) Bansal, V.; Patel, M. B.; Sarpal, A. S. Structural Aspects of Crude Oil Derived Asphaltenes by
1261 NMR and XRD and Spectroscopic Techniques. *Petroleum Science and Technology* **2004**, *22* (11-12),
1262 1401-1426. DOI: 10.1081/LFT-200027776.

1263 (48) Tanaka, R.; Sato, E.; Hunt, J. E.; Winans, R. E.; Sato, S.; Takanohashi, T. Characterization of
1264 Asphaltene Aggregates Using X-ray Diffraction and Small-Angle X-ray Scattering. *Energy & Fuels*
1265 **2004**, *18* (4), 1118-1125. DOI: 10.1021/ef034082z.

1266 (49) Andersen, S. I.; Jensen, J. O.; Speight, J. G. X-ray Diffraction of Subfractions of Petroleum
1267 Asphaltenes. *Energy & Fuels* **2005**, *19* (6), 2371-2377. DOI: 10.1021/ef050039v.

1268 (50) Trejo, F.; Ancheyta, J.; Morgan, T. J.; Herod, A. A.; Kandiyoti, R. Characterization of Asphaltenes
1269 from Hydrotreated Products by SEC, LDMS, MALDI, NMR, and XRD. *Energy & Fuels* **2007**, *21* (4),
1270 2121-2128. DOI: 10.1021/ef060621z.

1271 (51) Bouhadda, Y.; Bormann, D.; Sheu, E.; Bendedouch, D.; Krallafa, A.; Daaou, M. Characterization
1272 of Algerian Hassi-Messaoud asphaltene structure using Raman spectrometry and X-ray diffraction. *Fuel*
1273 **2007**, *86* (12), 1855-1864. DOI: <https://doi.org/10.1016/j.fuel.2006.12.006>.

1274 (52) Hoepfner, M. P.; Fogler, H. S. Multiscale Scattering Investigations of Asphaltene Cluster Breakup,
1275 Nanoaggregate Dissociation, and Molecular Ordering. *Langmuir* **2013**, *29* (49), 15423-15432. DOI:
1276 10.1021/la403531w.

1277 (53) AlHumaidan, F. S.; Hauser, A.; Rana, M. S.; Lababidi, H. M. S.; Behbehani, M. Changes in
1278 asphaltene structure during thermal cracking of residual oils: XRD study. *Fuel* **2015**, *150*, 558-564.
1279 DOI: <https://doi.org/10.1016/j.fuel.2015.02.076>.

1280 (54) Kananpanah, S.; Bayat, M.; Mousavian, M. A.; Solaimany Nazar, A. R. Impacts of physico-
1281 chemical properties of asphaltene aggregates on optimization of the thermal de-asphaltene process.
1282 *Journal of Petroleum Science and Engineering* **2016**, *147*, 718-725. DOI:
1283 <https://doi.org/10.1016/j.petrol.2016.09.018>.

1284 (55) Mousavi, M.; Pahlavan, F.; Oldham, D.; Abdollahi, T.; Fini, E. H. Alteration of intermolecular
1285 interactions between units of asphaltene dimers exposed to an amide-enriched modifier. *RSC Advances*
1286 **2016**, *6* (58), 53477-53492, 10.1039/C6RA07506A. DOI: 10.1039/C6RA07506A.

1287 (56) Kananpanah, S.; Kheirkhah, R.; Bayat, M.; Sadi, M.; Moosavian, M. A. Comparison of asphaltene
1288 structure and morphology under different deasphaltene methods. *Petroleum Science and Technology*
1289 **2017**, *35* (5), 457-464. DOI: 10.1080/10916466.2016.1258416.

1290 (57) Hemmati-Sarapardeh, A.; Dabir, B.; Ahmadi, M.; Mohammadi, A. H.; Husein, M. M. Toward
1291 mechanistic understanding of asphaltene aggregation behavior in toluene: The roles of asphaltene
1292 structure, aging time, temperature, and ultrasonic radiation. *Journal of Molecular Liquids* **2018**, *264*,
1293 410-424. DOI: <https://doi.org/10.1016/j.molliq.2018.04.061>.

1294 (58) Afra, S.; Nasr-El-Din, H. A.; Socci, D.; Cui, Z. Green phenolic amphiphile as a viscosity modifier
1295 and asphaltenes dispersant for heavy and extra-heavy oil. *Fuel* **2018**, *220*, 481-489. DOI:
1296 <https://doi.org/10.1016/j.fuel.2018.01.111>.

1297 (59) Gebresellasie, K.; Lewis, J. C.; Shirokoff, J. X-ray Spectral Line Shape Analysis of Asphalt
1298 Binders. *Energy & Fuels* **2013**, *27* (4), 2018-2024. DOI: 10.1021/ef301865p.

1299 (60) Sadeghtabghi, Z.; Rabbani, A. R.; Hemmati-Sarapardeh, A. Experimental evaluation of thermal
1300 maturity of crude oil samples by asphaltene fraction: Raman spectroscopy and X-ray diffraction.
1301 *Journal of Petroleum Science and Engineering* **2021**, *199*, 108269. DOI:
1302 <https://doi.org/10.1016/j.petrol.2020.108269>.

1303 (61) Wang, X.; Zhang, H.; Liang, X.; Shi, L.; Chen, M.; Wang, X.; Liu, W.; Ye, Z. New Amphiphilic
1304 Macromolecule as Viscosity Reducer with Both Asphaltene Dispersion and Emulsifying Capacity for
1305 Offshore Heavy Oil. *Energy & Fuels* **2021**, Article ASAP. DOI: 10.1021/acs.energyfuels.0c03256.

1306 (62) Alhreez, M.; Xiao, X.; Wen, D. Kinetic Study of Controlled Asphaltene Inhibitor Release from
1307 Nanoemulsions. *Langmuir* **2019**, *35* (33), 10795-10807. DOI: 10.1021/acs.langmuir.9b00481.

1308 (63) Eyssautier, J.; Espinat, D.; Gummel, J.; Levitz, P.; Becerra, M.; Shaw, J.; Barré, L. Mesoscale
1309 Organization in a Physically Separated Vacuum Residue: Comparison to Asphaltenes in a Simple
1310 Solvent. *Energy & Fuels* **2012**, *26* (5), 2680-2687. DOI: 10.1021/ef201411r.

1311 (64) Eyssautier, J.; Levitz, P.; Espinat, D.; Jestin, J.; Gummel, J.; Grillo, I.; Barré, L. Insight into
1312 Asphaltene Nanoaggregate Structure Inferred by Small Angle Neutron and X-ray Scattering. *The*
1313 *Journal of Physical Chemistry B* **2011**, *115* (21), 6827-6837. DOI: 10.1021/jp111468d.

1314 (65) Barré, L.; Jestin, J.; Morisset, A.; Palermo, T.; Simon, S. Relation between Nanoscale Structure of
1315 Asphaltene Aggregates and their Macroscopic Solution Properties. *Oil & Gas Science and Technology*
1316 *- Revue d'IFP Energies nouvelles* **2009**, *64* (5), 617-628. DOI: 10.2516/ogst/2009022 Ifp

1317 (66) Yang, Y.; Chaisoontornyotin, W.; Hoepfner, M. P. Structure of Asphaltenes during Precipitation
1318 Investigated by Ultra-Small-Angle X-ray Scattering. *Langmuir* **2018**, *34* (35), 10371-10380. DOI:
1319 10.1021/acs.langmuir.8b01873.

1320 (67) Barré, L.; Simon, S.; Palermo, T. Solution Properties of Asphaltenes. *Langmuir* **2008**, *24* (8), 3709-
1321 3717. DOI: 10.1021/la702611s.

1322 (68) Guinier, A.; Fournet, G.; Yudowitch, K. L. *Small-angle scattering of X-rays*; Wiley, 1955.

1323 (69) Ravey, J. C.; Ducouret, G.; Espinat, D. Asphaltene macrostructure by small angle neutron
1324 scattering. *Fuel* **1988**, *67* (11), 1560-1567. DOI: [https://doi.org/10.1016/0016-2361\(88\)90076-2](https://doi.org/10.1016/0016-2361(88)90076-2).

1325 (70) Sheu, E. Y.; Liang, K. S.; Sinha, S. K.; Overfield, R. E. Polydispersity analysis of asphaltene
1326 solutions in toluene. *Journal of Colloid and Interface Science* **1992**, *153* (2), 399-410. DOI:
1327 [https://doi.org/10.1016/0021-9797\(92\)90331-F](https://doi.org/10.1016/0021-9797(92)90331-F).

1328 (71) Zimm, B. H. The Scattering of Light and the Radial Distribution Function of High Polymer
1329 Solutions. *The Journal of Chemical Physics* **1948**, *16* (12), 1093-1099. DOI: 10.1063/1.1746738
1330 (accessed 2020/09/17).

1331 (72) Sheu, E. Y.; Storm, D. A.; De Tar, M. M. Asphaltenes in polar solvents. *Journal of Non-Crystalline*
1332 *Solids* **1991**, *131-133*, 341-347. DOI: [https://doi.org/10.1016/0022-3093\(91\)90326-2](https://doi.org/10.1016/0022-3093(91)90326-2).

1333 (73) Headen, T. F.; Boek, E. S.; Stellbrink, J.; Scheven, U. M. Small Angle Neutron Scattering (SANS
1334 and V-SANS) Study of Asphaltene Aggregates in Crude Oil. *Langmuir* **2009**, *25* (1), 422-428. DOI:
1335 10.1021/la802118m.

1336 (74) Storm, D. A.; Sheu, E. Y.; DeTar, M. M. Macrostructure of asphaltenes in vacuum residue by
1337 small-angle X-ray scattering. *Fuel* **1993**, *72* (7), 977-981. DOI: [https://doi.org/10.1016/0016-
1338 2361\(93\)90295-D](https://doi.org/10.1016/0016-2361(93)90295-D).

1339 (75) Sheu, E. Y. Small angle scattering and asphaltenes. *Journal of Physics: Condensed Matter* **2006**,
1340 *18* (36), S2485-S2498. DOI: 10.1088/0953-8984/18/36/s19.

1341 (76) Gawrys, K. L.; Blankenship, G. A.; Kilpatrick, P. K. Solvent Entrainment in and Flocculation of
1342 Asphaltenic Aggregates Probed by Small-Angle Neutron Scattering. *Langmuir* **2006**, *22* (10), 4487-
1343 4497. DOI: 10.1021/la052509j.

1344 (77) Gawrys, K. L.; Kilpatrick, P. K. Asphaltenic aggregates are polydisperse oblate cylinders. *Journal*
1345 *of Colloid and Interface Science* **2005**, *288* (2), 325-334. DOI:
1346 <https://doi.org/10.1016/j.jcis.2005.03.036>.

1347 (78) Roux, J.-N.; Broseta, D.; Demé, B. SANS Study of Asphaltene Aggregation: Concentration and
1348 Solvent Quality Effects. *Langmuir* **2001**, *17* (16), 5085-5092. DOI: 10.1021/la0101651.

1349 (79) Padula, L.; Balestrin, L. B. d. S.; Rocha, N. d. O.; de Carvalho, C. H. M.; Westfahl, H.; Cardoso,
1350 M. B.; Sabadini, E.; Loh, W. Role of Asphaltenes and Additives on the Viscosity and Microscopic
1351 Structure of Heavy Crude Oils. *Energy & Fuels* **2016**, *30* (5), 3644-3651. DOI:
1352 10.1021/acs.energyfuels.5b02103.

1353 (80) Kohlbrecher, J. User guide for the SASfit software package. *Paul Scherrer Institute* **2012**.

1354 (81) Liu, Y. C.; Sheu, E. Y.; Chen, S. H.; Storm, D. A. Fractal structure of asphaltenes in toluene. *Fuel*
1355 **1995**, *74* (9), 1352-1356. DOI: [https://doi.org/10.1016/0016-2361\(95\)00098-P](https://doi.org/10.1016/0016-2361(95)00098-P).

1356 (82) Duran, J. A.; Casas, Y. A.; Xiang, L.; Zhang, L.; Zeng, H.; Yarranton, H. W. Nature of Asphaltene
1357 Aggregates. *Energy & Fuels* **2019**, *33* (5), 3694-3710. DOI: 10.1021/acs.energyfuels.8b03057.

1358 (83) Dwiggin, C. W. A Small Angle X-Ray Scattering Study of the Colloidal Nature of Petroleum.
1359 *The Journal of Physical Chemistry* **1965**, *69* (10), 3500-3506. DOI: 10.1021/j100894a041.

1360 (84) Pollack, S. S.; Yen, T. F. Structural studies of asphaltics by x-ray small angle scattering. *Analytical*
1361 *Chemistry* **1970**, *42* (6), 623-629. DOI: 10.1021/ac60288a010.

1362 (85) Herzog, P.; Tchoubar, D.; Espinat, D. Macrostructure of asphaltene dispersions by small-angle X-
1363 ray scattering. *Fuel* **1988**, *67* (2), 245-250. DOI: [https://doi.org/10.1016/0016-2361\(88\)90271-2](https://doi.org/10.1016/0016-2361(88)90271-2).

1364 (86) Chang, C.-L.; Fogler, H. S. Stabilization of Asphaltenes in Aliphatic Solvents Using Alkylbenzene-
1365 Derived Amphiphiles. 2. Study of the Asphaltene-Amphiphile Interactions and Structures Using Fourier
1366 Transform Infrared Spectroscopy and Small-Angle X-ray Scattering Techniques. *Langmuir* **1994**, *10*
1367 (6), 1758-1766. DOI: 10.1021/la00018a023.

1368 (87) Xu, Y.; Koga, Y.; Strausz, O. P. Characterization of Athabasca asphaltenes by small-angle X-ray
1369 scattering. *Fuel* **1995**, *74* (7), 960-964. DOI: [https://doi.org/10.1016/0016-2361\(95\)00033-2](https://doi.org/10.1016/0016-2361(95)00033-2).

1370 (88) Fenistein, D.; Barré, L.; Frot, D. De l'agrégation à la floculation des asphaltènes, une description
1371 structurale par diffusion de rayonnement. *Oil & Gas Science and Technology - Rev. IFP* **2000**, *55* (1),
1372 123-128, 10.2516/ogst:2000006.

1373 (89) Fenistein, D.; Barré, L. Experimental measurement of the mass distribution of petroleum
1374 asphaltene aggregates using ultracentrifugation and small-angle X-ray scattering. *Fuel* **2001**, *80* (2),
1375 283-287. DOI: [https://doi.org/10.1016/S0016-2361\(00\)00072-7](https://doi.org/10.1016/S0016-2361(00)00072-7).

1376 (90) Savvidis, T. G.; Fenistein, D.; Barré, L.; Béhar, E. Aggregated structure of flocculated asphaltenes.
1377 *AIChE Journal* **2001**, *47* (1), 206-211. DOI: 10.1002/aic.690470120 (accessed 2020/10/26).

1378 (91) Cosultchi, A.; Bosch, P.; Lara, V. Small-angle X-ray scattering study of oil- and deposit-asphaltene
1379 solutions. *Colloid and Polymer Science* **2003**, *281* (4), 325-330. DOI: 10.1007/s00396-002-0772-2.

1380 (92) Espinat, D.; Fenistein, D.; Barré, L.; Frot, D.; Briolant, Y. Effects of Temperature and Pressure on
1381 Asphaltenes Agglomeration in Toluene. A Light, X-ray, and Neutron Scattering Investigation. *Energy*
1382 *& Fuels* **2004**, *18* (5), 1243-1249. DOI: 10.1021/ef030190+.

1383 (93) Tuzikov, F. V.; Larichev, Y. V.; Borisova, L. S.; Kozhevnikov, I. V.; Mart'yanov, O. N. Small-
1384 angle scattering study of colloidal particles in heavy crude oils. *Petroleum Chemistry* **2011**, *51* (4), 281.
1385 DOI: 10.1134/S0965544111040104.

1386 (94) Eyssautier, J.; Hénaut, I.; Levitz, P.; Espinat, D.; Barré, L. Organization of Asphaltenes in a
1387 Vacuum Residue: A Small-Angle X-ray Scattering (SAXS)–Viscosity Approach at High Temperatures.
1388 *Energy & Fuels* **2012**, *26* (5), 2696-2704. DOI: 10.1021/ef201412j.

1389 (95) Morimoto, M.; Imamura, H.; Shibuta, S.; Morita, T.; Nishikawa, K.; Yamamoto, H.; Tanaka, R.;
1390 Takanohashi, T. Asphaltene Aggregation Behavior in Bromobenzene Determined By Small-angle X-
1391 ray Scattering. *Energy & Fuels* **2015**, *29* (9), 5737-5743. DOI: 10.1021/acs.energyfuels.5b01491.

1392 (96) Larichev, Y. V.; Mart'yanov, O. N. The dynamics of asphaltene aggregates in heavy crude oils on
1393 a nanometer scale studied via small-angle X-ray scattering in situ. *Journal of Petroleum Science and*
1394 *Engineering* **2018**, *165*, 575-580. DOI: <https://doi.org/10.1016/j.petrol.2018.02.063>.

1395 (97) Larichev, Y. V.; Kovalenko, E. Y.; Mart'yanov, O. N. Effect of Nitrogen Bases on the Structure
1396 of Primary Asphaltene Clusters and Dynamics of Aggregation of Heavy Oil Fractions. *Petroleum*
1397 *Chemistry* **2019**, *59* (11), 1195-1200. DOI: 10.1134/S0965544119110100.

1398 (98) Ismail, M.; Yang, Y.; Chaisoontornytin, W.; Ovalles, C.; Rogel, E.; Moir, M. E.; Hoepfner, M.
1399 P. Effect of Chemical Inhibitors on Asphaltene Precipitation and Morphology Using Ultra-Small-Angle
1400 X-ray Scattering. *Energy & Fuels* **2019**, *33* (5), 3681-3693. DOI: 10.1021/acs.energyfuels.8b03055.

1401 (99) Thiyagarajan, P.; Hunt, J. E.; Winans, R. E.; Anderson, K. B.; Miller, J. T. Temperature-Dependent
1402 Structural Changes of Asphaltenes in 1-Methylnaphthalene. *Energy & Fuels* **1995**, *9* (5), 829-833. DOI:
1403 10.1021/ef00053a014.

1404 (100) Fenistein, D.; Barré, L.; Broseta, D.; Espinat, D.; Livet, A.; Roux, J.-N.; Scarsella, M.
1405 Viscosimetric and Neutron Scattering Study of Asphaltene Aggregates in Mixed Toluene/Heptane
1406 Solvents. *Langmuir* **1998**, *14* (5), 1013-1020. DOI: 10.1021/la9709148.

1407 (101) Tanaka, R.; Hunt, J. E.; Winans, R. E.; Thiyagarajan, P.; Sato, S.; Takanoashi, T. Aggregates
1408 Structure Analysis of Petroleum Asphaltenes with Small-Angle Neutron Scattering. *Energy & Fuels*
1409 **2003**, *17* (1), 127-134. DOI: 10.1021/ef020019i.

1410 (102) Gawrys, K. L.; Matthew Spiecker, P.; Kilpatrick, P. K. The Role of Asphaltene Solubility and
1411 Chemical Composition on Asphaltene Aggregation. *Petroleum Science and Technology* **2003**, *21* (3-4),
1412 461-489. DOI: 10.1081/LFT-120018533.

1413 (103) Hoepfner, M. P.; Vilas Bôas Fávero, C.; Haji-Akbari, N.; Fogler, H. S. The Fractal Aggregation
1414 of Asphaltenes. *Langmuir* **2013**, *29* (28), 8799-8808. DOI: 10.1021/la401406k.

1415 (104) Ballard, D. A.; Qiao, P.; Cattoz, B.; Dowding, P. J.; Prevost, S.; Alshamsi, M.; Charpentier, T.;
1416 Roberts, K. J.; Xu, Z.; Harbottle, D. Aggregation Behavior of E-SARA Asphaltene Fractions Studied
1417 by Small-Angle Neutron Scattering. *Energy & Fuels* **2020**, *34*, 6894–6903. DOI:
1418 10.1021/acs.energyfuels.0c00596.

1419 (105) Knudsen, K. D.; Simon, S.; Geue, T.; Cooper, J. F. K.; Sjöblom, J. Interactions between
1420 Asphaltenes and a Model Demulsifier in Bulk and at an Interface Studied by Small-Angle Neutron
1421 Scattering (SANS) and Neutron Reflectometry. *Energy & Fuels* **2020**, *34* (6), 6768-6779. DOI:
1422 10.1021/acs.energyfuels.9b03831.

1423 (106) Beaucage, G. Small-Angle Scattering from Polymeric Mass Fractals of Arbitrary Mass-Fractal
1424 Dimension. *Journal of Applied Crystallography* **1996**, *29* (2), 134-146. DOI:
1425 10.1107/S0021889895011605 (accessed 2020/10/26).

1426 (107) Heenan, R. K. "Fish" Data Analysis Program; Rutherford Appleton Laboratory, 1989.

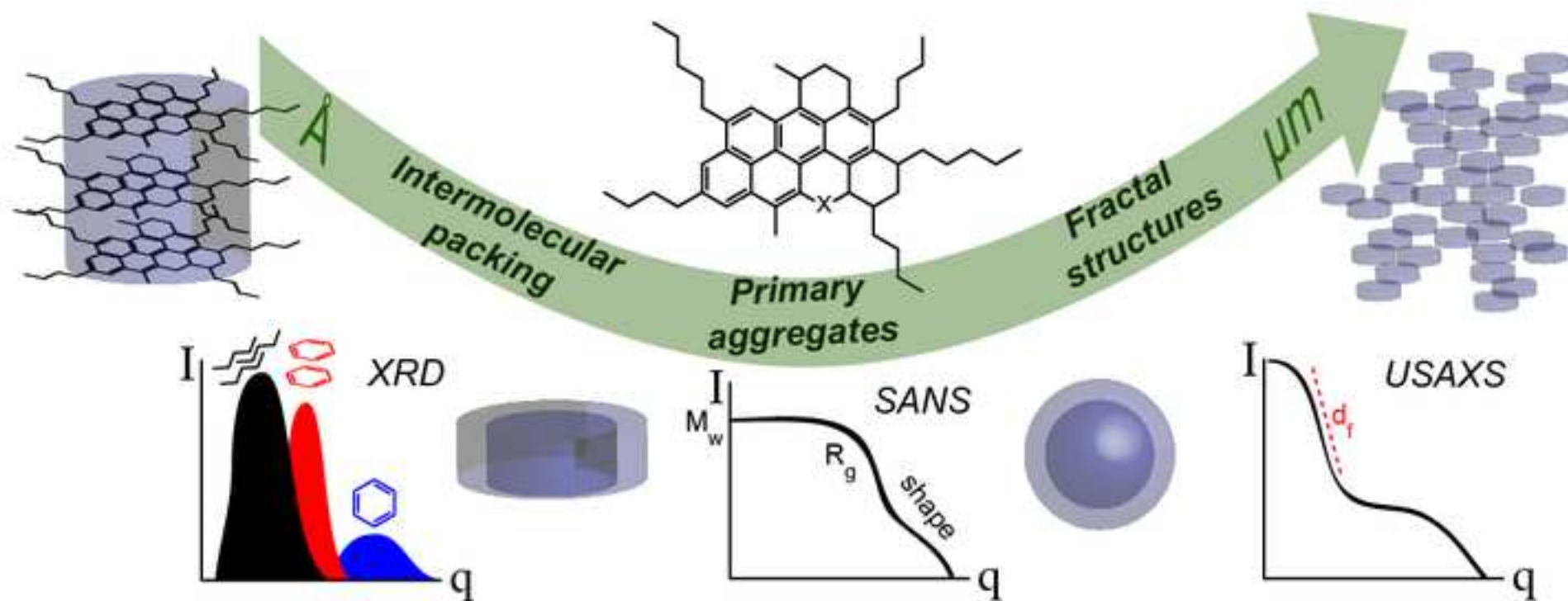
1427 (108) González, G.; Middea, A. Peptization of asphaltene by various oil soluble amphiphiles. *Colloids*
1428 *and Surfaces* **1991**, *52*, 207-217. DOI: [https://doi.org/10.1016/0166-6622\(91\)80015-G](https://doi.org/10.1016/0166-6622(91)80015-G).

1429 (109) Al-Sahhaf, T. A.; Fahim, M. A.; Elkilani, A. S. Retardation of asphaltene precipitation by addition
1430 of toluene, resins, deasphalted oil and surfactants. *Fluid Phase Equilibria* **2002**, 194-197, 1045-1057.
1431 DOI: [https://doi.org/10.1016/S0378-3812\(01\)00702-6](https://doi.org/10.1016/S0378-3812(01)00702-6).

1432

1433

1434



Declaration of interests

The authors declare that they have no known competing financial interests or personal relationships that could have appeared to influence the work reported in this paper.

The authors declare the following financial interests/personal relationships which may be considered as potential competing interests: